A&A 516, A85 (2010)
DOI: 10.1051/0004-6361/200913429

Astronomy & Astrophysics

A close look at the Centaurus A group of galaxies

I. Metallicity distribution functions and population gradients in early-type dwarfs

D. Crnojević[1,⋆], E. K. Grebel[1], and A. Koch[2]

[1] Astronomisches Rechen-Institut, Zentrum für Astronomie der Universität Heidelberg, Mönchhofstrasse 12-14, 69120 Heidelberg, Germany
e-mail: denija@ari.uni-heidelberg.de
[2] Department of Physics and Astronomy, University of Leicester, University Road, Leicester LE1 7RH, UK

Received 8 October 2009 / Accepted 26 January 2010

ABSTRACT

Aims. We study dwarf galaxies in the Centaurus A group to investigate their metallicity and possible environmental effects. The Centaurus A group (at ∼4 Mpc from the Milky Way) contains about 50 known dwarf companions of different morphologies and stellar contents, thus making it a very interesting target to study how these galaxies evolve.
Methods. Here we present results for the early-type dwarf galaxy population in this group. We used archival HST/ACS data to study the resolved stellar content of 6 galaxies, together with isochrones from the Dartmouth stellar evolutionary models.
Results. We derive photometric metallicity distribution functions of stars on the upper red giant branch via isochrone interpolation. The 6 galaxies are moderately metal-poor ($\langle$[Fe/H]$\rangle$ = −1.56 to −1.08), and metallicity spreads are observed (internal dispersions of σ[Fe/H] = 0.10–0.41 dex). We also investigate whether intermediate-age stars are present, and discuss how these affect our results. The dwarfs exhibit flat to weak radial metallicity gradients. For the two most luminous, most metal-rich galaxies, we find statistically significant evidence of at least two stellar subpopulations: the more metal-rich stars are found in the center of the galaxies, while the metal-poor ones are more broadly distributed within the galaxies.
Conclusions. We find no clear trend in the derived physical properties as a function of (present-day) galaxy position in the group, which may come from the small sample we investigate. We compare our results to the early-type dwarf population of the Local Group, and find no outstanding differences, even though the Centaurus A group is a denser environment that is possibly in a more advanced dynamical stage.

Key words. galaxies: dwarf – galaxies: evolution – galaxies: photometry – galaxies: groups: individual: CenA group – galaxies: stellar content

1. Introduction

Dwarf galaxies are fundamental ingredients for assembling luminous structures in our Universe. They may be the smallest baryonic counterparts of dark matter subhalo building blocks in a ΛCDM cosmology, and appear to be the most dark matter dominated objects in the Universe (see e.g. Gilmore et al. 2007). Although their role is still under debate, it is certain that they are the most numerous type of galaxy, and an increasing number of them are being discovered with current state-of-the-art surveys (see e.g. Belokurov et al. 2006; Zucker et al. 2006a,b, 2007). It is thus interesting to study their physical properties to gain a deeper understanding of how galaxies evolve and of the main processes that drive this evolution.

Dwarf galaxies in groups have been looked at in detail in the past decade (e.g., Trentham & Tully 2002; Karachentsev et al. 2004; Karachentsev 2005; Grebel 2007; Sharina et al. 2008; Weisz et al. 2008; Bouchard et al. 2009; Dalcanton et al. 2009; Koleva et al. 2009). The main purpose of most of these studies was to catalog and characterize new objects in nearby groups and to look for possible environmental effects on galaxy evolution (see Grebel et al. 2000, for details). The largest amount of information is, of course, coming from our own Local Group, for which very deep observations permit us both to have a broad and detailed view of the physical properties of dwarf galaxies and to investigate how they form and evolve in this type of environment (Grebel 1997; Mateo 1998; van den Bergh 1999; Tolstoy et al. 2009).

In Local Group dwarf galaxies, all of the morphological types contain old populations, even though their fractions differ (e.g. Grebel 1997; Mateo 1998; Grebel et al. 2003; Tolstoy et al. 2009). The old populations (≳10 Gyr) in the classical dwarf spheroidal companions of the Milky Way seem to have a common age within the accuracy of photometric age-dating techniques (Grebel & Gallagher 2004). The main difference between early-type (spheroidal and elliptical) dwarfs and late-type (irregular) dwarfs is that only the latter contain large amounts of neutral gas and formed stars throughout their whole history. Moreover, dwarf galaxies both in the Local Group and in other groups follow the general morphology-density relation that holds in dense environments (e.g. Einasto et al. 1974; Dressler 1980; Karachentsev et al. 2002). This means that early-type dwarfs are normally found within ∼300 kpc of the center of the dominant galaxies in the group, while late-type dwarfs are more widely distributed.

The chemical composition of stars in early-type dwarfs (i.e., faint dwarf spheroidals and dwarf ellipticals, the latter showing

⋆ Member of IMPRS (International Max Planck Research School) for Astronomy & Cosmic Physics at the University of Heidelberg and of the Heidelberg Graduate School for Fundamental Physics.

higher central surface brightnesses and more elongated shapes) has been well studied with detailed spectroscopic and kinematic data. All these dwarfs are metal-poor and show wide metallicity spreads (e.g., Shetrone et al. 2001; Sarajedini et al. 2002; Tolstoy et al. 2004; Battaglia et al. 2006; Helmi et al. 2006; Koch et al. 2006; Bosler et al. 2007; Koch et al. 2007a,b; Gullieuszik et al. 2009). Their metallicity distribution functions (MDFs) often show a slow increase toward higher metallicities and then a steeper decline (see Koch et al. 2007a), but there are many individual differences reflecting a wide range of complex star formation histories (e.g., Grebel 1997; Tolstoy et al. 2009). Occasionally there is evidence of intermediate-age and even younger populations (e.g., in the dwarf spheroidals Fornax and Carina). Detailed models of chemical evolution have been developed and applied to dwarf spheroidals in our Local Group (e.g., Lanfranchi & Matteucci 2004; Marcolini et al. 2006; Marcolini et al. 2008; Revaz et al. 2009), and they are able to reproduce the shape of the observed MDFs. The above-mentioned asymmetry of the MDFs with a steeper fall-off on the metal-rich side may be explained by an evolution that is regulated by supernova explosions and stellar winds (e.g., Dekel & Silk 1986; Lanfranchi & Matteucci 2004).

Previous studies have also looked at possibly distinct stellar spatial distributions of different stellar populations in early-type dwarf galaxies (e.g., Stetson et al. 1998; Hurley-Keller et al. 1999). The first systematic study of a large sample of dwarfs was carried out by Harbeck et al. (2001), who investigated morphological gradients based on horizontal branch and RGB stars for a sample of 9 galaxies. They showed that if gradients are present they are always such that the more metal-rich and/or younger populations are more centrally concentrated. Later on, spectroscopic studies were able to also confirm chemically, and in some cases also kinematically, distinct subpopulations for various dwarfs, like Fornax, Sculptor, and Sextans (e.g., Tolstoy et al. 2004). However, there are also cases for which such distinct populations were not found, but only weak metallicity gradients as a function of radius were present (e.g., Harbeck et al. 2001; Koch et al. 2006, 2007a,b).

It is then interesting to extend our knowledge to dwarf galaxies in other groups to be able to draw general conclusions about dwarf galaxy properties in different environments. Do loose, filamentary structures (like the Canes Venatici cloud or the Sculptor group, see Karachentsev et al. 2003a,c) have similar properties in their galaxy populations to the denser, more evolved groups we know (the Local Group itself, or the Centaurus A group, e.g., Karachentsev et al. 2002), or are there striking differences in the way they spend their lives? Future studies should be able to answer this and many further questions by looking closely at nearby groups, and comparing them to what we already know about our own.

The currently available telescopes and instruments permit us not only to substantially improve the census of galaxies in nearby groups, but also to derive their detailed photometric properties, providing new insight into a range of physical properties for these objects. In particular, the deep high-resolution images from the Hubble Space Telescope (HST) are now providing optically resolved stellar populations in dwarfs within ~10 Mpc from the Local Group. Even though the limiting absolute magnitude dramatically decreases with their distance, we can still observe these galaxies down to comparable sensitivity levels as we used to see much closer dwarf galaxies in our own Local Group, as recently as only a decade ago (e.g., Dohm-Palmer et al. 1997).

The Centaurus A group is located in the southern hemisphere, at an average Galactic latitude of $b \sim 20°$. Despite this low latitude, most of its members are not highly contaminated by Galactic foreground extinction (see, e.g., Schlegel et al. 1998), making it a very popular target of research. It is one of the closest groups to our own, with a mean Galactocentric distance of ~3.8 Mpc (Hui et al. 1993; Karachentsev et al. 2002, 2007; Harris et al. 2009) and with a variety of morphological types among its member galaxies. The group is dominated by the giant radio-loud elliptical galaxy Centaurus A (NGC 5128), which shows a very perturbed morphology and which has probably undergone several mergers in its recent past (e.g., Meier et al. 1989; Mirabel et al. 1999; Karachentsev 2005). Within the Centaurus A group, there is a subgroup centered on the spiral galaxy M 83 (NGC 5236), even though it is not clear whether this subgroup is approaching or receding from Centaurus A (e.g. Karachentsev et al. 2007). The search for and study of dwarf members in this group have been pursued at different wavelengths for more than a decade (Côté et al. 1997; Karachentseva & Karachentsev 1998; Banks et al. 1999; Côté et al. 2000; Jerjen et al. 2000a,b; Karachentsev et al. 2002, 2004; Karachentsev 2005; Rejkuba et al. 2006; Bouchard et al. 2007; Grossi et al. 2007; Karachentsev et al. 2007; Lee et al. 2007; Bouchard et al. 2009; Côté et al. 2009). Now there are more than 50 confirmed dwarf galaxies known in the Centaurus A group, of which about 3/5 are early-type dwarfs. When looking at the luminosity function of the entire group, we note that there are more luminous early-type dwarfs than in our own Local Group or in the Sculptor group, as expected for a more evolved group (Jerjen et al. 2000a). However, many more faint early-type dwarfs could possibly be found if more sensitive surveys were available. In particular, we know now that the Local Group contains about 20 dwarfs with $M_B > -10$, while, due to its distance, only 4 such faint objects have been detected so far in the Centaurus A group.

Some of the galaxies presented here have already been investigated in previous studies (e.g. Côté et al. 1997; Jerjen et al. 2000a; Bouchard et al. 2007, 2009; Côté et al. 2009), in some cases even with the same dataset considered in our work (Karachentsev et al. 2007; Makarova & Makarov 2008; Sharina et al. 2008). However, most of these studies concentrated on large samples of objects and did not investigate their physical properties individually. Bouchard et al. (2007) find that in the Centaurus A group there is an apparent gap in HI masses: the detected galaxies have gas masses of about $10^7\ M_\odot$, or they are not detected at all (which permits them to put an upper limit of $\sim 10^6\ M_\odot$). Bouchard et al. (2007) conclude that the Centaurus A group environment must favor an efficient gas stripping from its dwarf companions. However, they also point out that the limits of the HI survey make it currently impossible to detect so-called mixed-type dwarfs in the Centaurus A group (with no ongoing star formation but with neutral gas). Thus, knowledge of only the stellar content of early-type dwarfs does not tell us with certainty whether they are "contaminated" by residual gas. Bouchard et al. (2009) have collected literature data for dwarfs in the Centaurus A and Sculptor groups and analyzed them along with new observations. Again, there is no significant ongoing star formation for early-type galaxies. Bouchard et al. (2009) investigate the dependence of several physical properties (optical luminosity, neutral gas and Hα content) on environment. In a similar way to the Local Group, they are able to confirm: that galaxies in denser regions of these groups have, in general, lower values of HI; that the star formation in these objects is lower; and that they probably formed their stellar content earlier, with respect to galaxies in low-density regions. However, these correlations with environment do not rule out the simultaneous

impact of internal processes that act to shape their evolution. The papers that use the same dataset as in our study mostly consider distances (Karachentsev et al. 2007) or scaling relations (Sharina et al. 2008) for an extensive sample of dwarfs in the Centaurus A group, and dwarfs in nearby groups and in the field. In our work we want to look in more detail at the metallicity and population gradients of early-type dwarfs in the Centaurus A group.

This paper is the first in a series in which we concentrate on the resolved stellar populations of dwarf galaxies in the Centaurus A group, seen through the Hubble Space Telescope. We derive their physical properties (metallicities, star formation rates, stellar spatial distributions) and try to find links with the environment they reside in, in order to put constraints on their evolution. While this paper focuses on the early-type dwarfs, we will return to the late type dwarf irregular dwarfs in two forthcoming papers (Crnojević et al., in prep.).

The paper is organized as follows. We describe the data in Sect. 2, and present the derived results in Sect. 3 (color–magnitude diagrams), Sects. 4 and 5 (metallicity distribution functions and discussion of their uncertainties, respectively), Sect. 6 (metallicity and population gradients). The discussion is then carried out in Sect. 7, and our conclusions are drawn in Sect. 8.

2. Data and photometry

We use archival data obtained with the Wide Field Channel (WFC) of the Advanced Camera for Surveys (ACS) aboard the Hubble Space Telescope (HST). Observations with this instrument are available for 21 dwarfs in the CenA group (programes GO-9771 and GO-10235). Each galaxy has a 1200 s exposure in the $F606W$ filter and a 900 s exposure in the $F814W$ filter. We do not consider observations carried out with the Wide Field Planetary Camera 2 (WFPC2), since its field of view is smaller, three of its chips have lower resolution and it is less sensitive than the ACS. Earlier studies of dwarfs in the Centaurus A group based on WFPC2 data were published by, e.g., Karachentsev et al. (2002, 2003b); Rejkuba et al. (2006). In this paper we present the results for 6 early-type dwarf galaxy companions of the peculiar elliptical Centaurus A. Another sample of 11 late-type dwarfs (6 companions of Centaurus A and 5 of the giant spiral galaxy M 83, respectively) will be studied in two forthcoming papers of this series.

We performed stellar photometry using the ACS module of the DOLPHOT package (Dolphin 2002), as described in detail in, for instance, Dalcanton et al. (2009). The parameters chosen for the photometry follow the prescriptions of the DOLPHOT User's Guide[1]. The stars that we then want to retain from the original photometry have to simultaneously satisfy the required cuts for different quality parameters in both wavelengths. These limits are the following: each object must be classified as a good star, meaning a not too extended or too sharp an object, which is quantified by an "object type" that has to be ≤2. Moreover, each object has to be recovered extremely well in the image, i.e. we require the "error flag" to be 0 in order to avoid saturation or photometry extending out of the chip. The object's signal-to-noise ratio has to be at least 5, its sharpness parameter has to be $|sharp| \leq 0.3$, the crowding parameter is set to a value lower than 0.5 (in mag, which quantifies how much brighter the star would be if isolated when measured), and finally the χ has to be ≤2.5. This selection choice leaves us with fairly clean color–magnitude diagrams. For the following study, we use the V and I-bands, converted by the DOLPHOT program from the instrumental magnitudes with the prescriptions of Sirianni et al. (2005).

Extensive artificial star tests were then run with the same package to estimate the photometric uncertainties and to assess the incompleteness effects. For each galaxy, we add ∼5 times the number of observed stars to the images (after quality cuts). The artificial stars we added are measured one at a time by the DOLPHOT routine, in order to avoid artificial crowding. They are distributed evenly across the field of view of ACS, and have a magnitude range that goes from the brightest observed stars' magnitude to ∼1 mag fainter than the faintest ones (to account for fainter stars possibly upscattered in the color–magnitude diagram by noise). The color range is the same as for the observed stars. After running the photometry again with the artificial stars, we applied the same quality cuts as before. We then derived completeness curves as a function of both magnitude and radius, in order to correct star number counts (see Sect. 6). The limiting magnitude, taken at a 50% completeness level, is at ∼27.3 (∼26.8) mag in the V-band for the least (most) crowded objects of our sample, and at ∼26.4 (∼26.0) mag in the I-band. The mentioned galaxies are KKS55 and ESO269-66 (as can be seen from the density maps reported in Sect. 6), with peak stellar densities of ∼39 and ∼124 stars per 0.01 kpc^2. At a completeness level of 50%, the 1σ extremes of the photometric errors amount to ≤0.23 mag (≤0.16 mag) in I-band magnitude and ≤0.30 mag (≤0.21 mag) in color, for these two galaxies. The mean photometric errors (±1σ) for each galaxy are indicated by representative errorbars in the color–magnitude diagrams shown in Sect. 3.

The main properties of the galaxies studied here are listed in Table 1 as follows: Col. (1): name of the galaxy; (2–3): equatorial coordinates (J2000); (4): morphological type; (5): I-band magnitude at the tip of the red giant branch (from Karachentsev et al. 2007); (6): distance of the galaxy derived by Karachentsev et al. (2007) with the tip of the red giant branch method; (7): foreground extinction in the I-band from Schlegel et al. (1998); (8): absolute B magnitude from Karachentsev (2005); (9): absolute V magnitude from Georgiev et al. (2008); and (10): tidal index, taken from Karachentsev et al. (2007).

3. Color magnitude diagrams

The color–magnitude diagrams (CMDs) of the six galaxies are shown in Fig. 1, ordered by increasing absolute V magnitude of the galaxies. The CMDs all show prominent red giant branches (RGBs), where stars may encompass a wide range of ages, starting with ages as young as 1–2 Gyr. Populations with ages of a few Gyr ("intermediate-age stars", 1–9 Gyr) can be recognized by several additional features including more luminous main sequence turnoffs, red clump and vertical red clump stars, and luminous asymptotic giant branch (AGB) stars with luminosities greater than the tip of the RGB (TRGB). Unfortunately, the HST data are not deep enough to reach the main sequence turnoffs or the red clump stars of the intermediate-age populations, as these are below our detection limit of ∼27 I-band apparent magnitude (the red clump would be expected to have a magnitude of ∼28 in the same band). However, we can infer the presence or absence of intermediate-age populations from the presence or absence of luminous AGB stars. Even younger stars (<1 Gyr) are definitely not present in these galaxies, as there are no objects found in the region blueward of the RGB (i.e., upper main sequence, or massive blue and red He-burning stars). A quantitative evaluation of the amount of intermediate-age stars, and how it affects our results, is presented in Sect. 6. Similar evidence of

[1] http://purcell.as.arizona.edu/dolphot/

Table 1. Fundamental properties of our sample of galaxies.

Galaxy	RA (J2000)	Dec (J2000)	T	$I_{\rm TRGB}$	D (Mpc)	A_I	M_B	M_V	Θ
KK189	13 12 45.0	−41 49 55	−3	24.40 ± 0.07	4.42 ± 0.33	0.22	−10.52	−11.99	2.0
ESO269-66, KK190	13 13 09.2	−44 53 24	−5	24.04 ± 0.04	3.82 ± 0.26	0.18	−13.85	−13.89	1.7
KK197	13 22 01.8	−42 32 08	−3	24.19 ± 0.04	3.87 ± 0.27	0.30	−12.76	−13.04	3.0
KKs55	13 22 12.4	−42 43 51	−3	24.21 ± 0.03	3.94 ± 0.27	0.28	−9.91	−11.17	3.1
KKs57	13 41 38.1	−42 34 55	−3	24.10 ± 0.05	3.93 ± 0.28	0.18	−10.07	−10.73	1.8
CenN	13 48 09.2	−47 33 54	−3	24.10 ± 0.04	3.77 ± 0.26	0.27	−10.89	−11.15	0.9

Notes. Units of right ascension are hours, minutes, and seconds, and units of declination are degrees, arcminutes, and arcseconds. The references for the reported values are Karachentsev (2005) and Karachentsev et al. (2007), and Georgiev et al. (2008) for the absolute V magnitude.

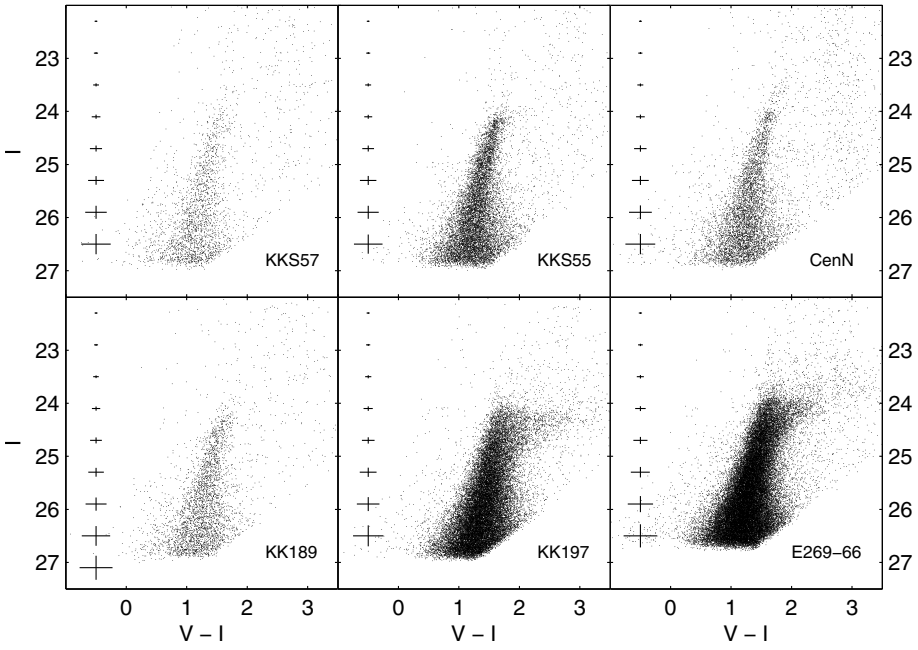

Fig. 1. Color–magnitude diagrams of the six early-type dwarf galaxies studied in this paper, ordered by absolute V magnitude of the galaxies. The main feature visible in all of the CMDs is a prominent RGB, while luminous AGB stars are less numerous (see text for an estimate for each galaxy). Representative errorbars derived from artificial star experiments are shown on the left side of the diagrams. At an I-band magnitude of 25.5, the 1σ photometric errors are ∼0.1 mag in magnitude and ∼0.15 mag in color (see text for details).

intermediate-age components has also been found in some of the dwarf spheroidals and dwarf ellipticals of the Local Group, such as Leo I, Leo II, Fornax, Carina, NGC 147, and NGC 185 (e.g., Han et al. 1997).

In the CMDs of Fig. 1, we also show representative photometric errors derived from artificial star tests. The (1σ) error is ∼0.1 mag in magnitude and ∼0.15 mag in color at an I-band magnitude of 25.60 for KKS57, 25.55 for KKS55, 25.50 for CenN, 25.55 for KK189, 25.45 for KK197 and 25.30 for ESO269-66. The RGB is thus partly broadened by photometric errors in the observed CMDs. However, the broadening does not come entirely from the errors, so is also associated with the physical properties of the galaxies. In particular, the color spread across the RGB could stem from either age or metallicity. There is a well known degeneracy in this evolutionary stage, such that stars that are younger and more metal-rich may be found in the same RGB region as stars that are older and more metal-poor. Ideally, for a "simple" stellar population a spread in age would produce a narrower RGB at the same metallicity than would a spread in metallicity at a constant age (see, for example, VandenBerg et al. 2006). Owing to the relatively small number of luminous AGB stars above the TRGB, we may assume that the majority of the RGB stars belong to old populations (10 Gyr or older). Because of this, and also because early-type dwarfs in the Local Group all display metallicity spreads, we assume that the color spread across the RGB is predominantly caused by a metallicity range within these galaxies. Our goal is then to derive photometric metallicity distribution functions from the CMDs.

We want to stress that a spread in metallicity would imply the presence of an age spread as well (∼1–2 Gyr), such that the first generation of stars born in the galaxy would have time to evolve and pollute the surrounding interstellar medium, making it possible for the next star formation episodes to produce more metal-rich stars. This spread at such old ages is, however, not resolvable from the upper part of the RGB alone, and from our data we can only try to put some constraints on the age range of the intermediate-age populations from the number and brightness of the luminous AGB stars. The unresolvable spread in age for old populations could have the effect of inflating the derived metallicity spreads by 10–20%. On the other side, the possible presence of intermediate-age stars would also affect the metallicity spreads in a way that depends on each individual galaxy's characteristics, and it deserves more careful attention. Both these aspects will be discussed in detail in the next section.

4. Metallicity distribution functions

At the distance of the Centaurus A group (∼3.8 Mpc on average, Karachentsev et al. 2007), there is no possibility of obtaining individual stellar absorption line spectra for red giants using the current instrumentation within reasonable integration times (compare $I_{\rm TRGB}$ in Table 1). Moreover, genuine early-type dwarf

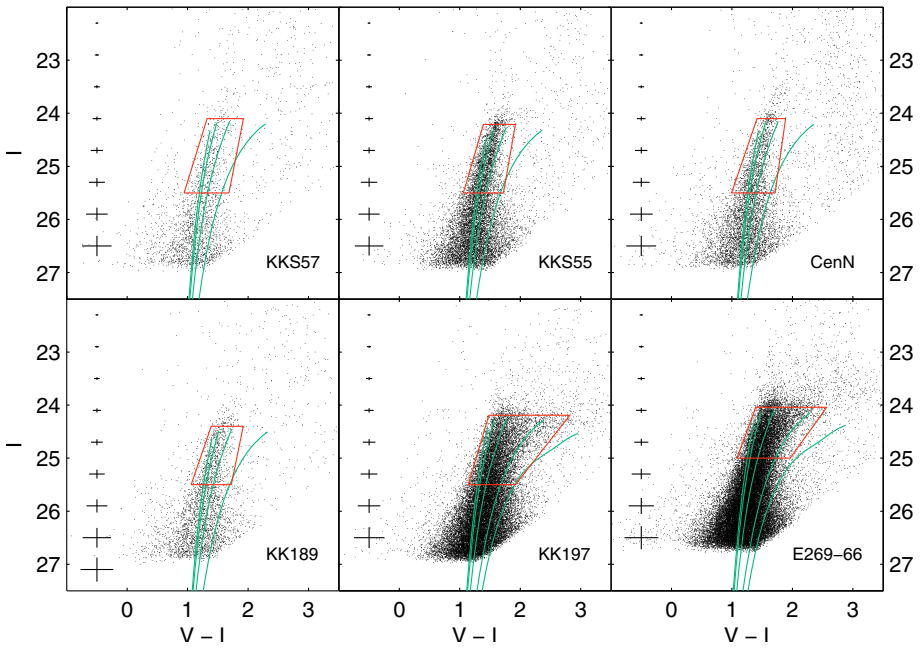

Fig. 2. Color–magnitude diagrams of the six early-type dwarf galaxies studied in this paper, ordered by absolute V magnitude of the galaxies, as in Fig. 1. Overlaid are Dartmouth stellar isochrones (green solid lines) with a fixed age of 10 Gyr, shifted to the distance of the galaxies and reddened according to the values listed in Table 1. Their metallicities have values of [Fe/H] = −2.5, −1.9, −1.3 and −0.7 (proceeding from the blue to the red parts of the CMD). For KK197 and ESO269-66, the isochrone with [Fe/H] = −0.4 is also shown, because of the broader RGB. Drawn in red is the selection box within which we interpolate metallicity values for the single RGB stars (see text for details).

galaxies usually do not contain neutral gas reservoirs or show ongoing star formation. As a result, we cannot directly measure their present-day metallicity from spectroscopy of HII regions around massive young stars. Finally, a reconstruction of the star formation history from CMDs would be almost impossible, given the small amount of information that comes from the RGBs alone.

The only tool we have for constraining metallicity in this type of galaxy and at these distances, is thus photometry combined with isochrones. Once we have a set of isochrones from an evolutionary model, we can overlay them on the observed CMDs, as shown in Fig. 2. In the case of a single stellar population with a narrow RGB, one would try to find the one best-fitting isochrone. However, early-type dwarf galaxies, at least in the Local Group, are known to have wide spreads in their metallicities (e.g., Grebel 1997; Mateo 1998). As our RGBs look quite broad and there are no young population features in the CMDs (i.e., stars younger than ∼1 Gyr, as argued in the previous section), we make the simplified assumption of a single, fixed old age and then let the metallicity of the isochrones vary to cover the whole RGB color range. In this way we are able to derive the metallicity of each star on the RGB via interpolation among the isochrones. This method is widely used for studies of predominantly old populations, for which spectroscopy is not available (e.g., Durrell et al. 2001; Sarajedini et al. 2002; Rejkuba et al. 2005; Harris et al. 2007; Richardson et al. 2009), to derive photometric metallicity distribution functions.

In this method, there are some weaknesses that have to be taken into account. First, we have a small (∼22%, see e.g. Durrell et al. 2001) contamination from old (≳10 Gyr), low-luminosity AGB stars that overlap with our RGB. With the available photometry it is impossible to distinguish them from RGB stars, and our main conclusions are not affected by this inevitable contamination since it would introduce a systematic bias towards slightly lower metallicities within the investigated metallicity range. That is, we would have an approximately equally overestimated numer of stars for each metallicity bin. Second, we observe luminous AGB stars above the TRGB, which resemble an intermediate-age, metal-poor population (going up almost straight to higher luminosities), meaning that there will be a non-negligible contribution from these stars in the most metal-poor bins of our resulting metallicity distribution functions. This effect has to be quantified more accurately for each galaxy and is considered in the next section.

In Fig. 2 we overplot on the observed CMDs the boxes (in red) used to select the putative stars for which we derive metallicities. Their width in color is chosen by constructing Hess diagrams for the galaxies, so as to approximately contain stars that lie within $\sim\pm3\sigma$ from the mean locus of the RGB. Their vertical size is such that the stars in the selection boxes have 1σ photometric errors of ≤0.1 mag in magnitude and ≤0.15 mag in color, and go up to the TRGB (the apparent magnitude of the latter has been adopted from Karachentsev et al. 2007). In the selected region, the I-band completeness is above the ∼70% level and the theoretical isochrones are more widely separated from each other than at lower luminosities, providing a better resolution in metallicity.

In Fig. 2 we further show the adopted stellar isochrones, taken from the Dartmouth evolutionary models (Dotter et al. 2008). We chose not to use α-enhanced tracks, because nothing is known about the level of the α-enhancements in our target galaxies. The effects of this arbitrary choice will be discussed in the next section. The isochrones are shifted to the distance of each observed galaxy and reddened by the respective foreground reddening value. Distances and reddening values are taken from Karachentsev et al. (2007) and from the Schlegel extinction maps (Schlegel et al. 1998), respectively. The Dartmouth set of evolutionary models is able to reproduce particularly well the populations of old and intermediate-age clusters, while other models generally fail to simultaneously reproduce all features of the CMD for the correct, spectroscopically measured metallicity (e.g., Glatt et al. 2008a,b; Sarajedini et al. 2009). We choose a fixed age of 10 Gyr, and metallicities ranging from [Fe/H] = −2.5 to −0.3 in solar units. The implications of this simplistic, single age assumption are discussed in detail in the next section. The isochrone grid is finely spaced (0.2 dex steps), in order to get good interpolation values for each star. We interpolate linearly among the isochrones. We also only retain stars that fall within the range of our isochrone grid, while rejecting those with extrapolated values (meaning values blueward of the

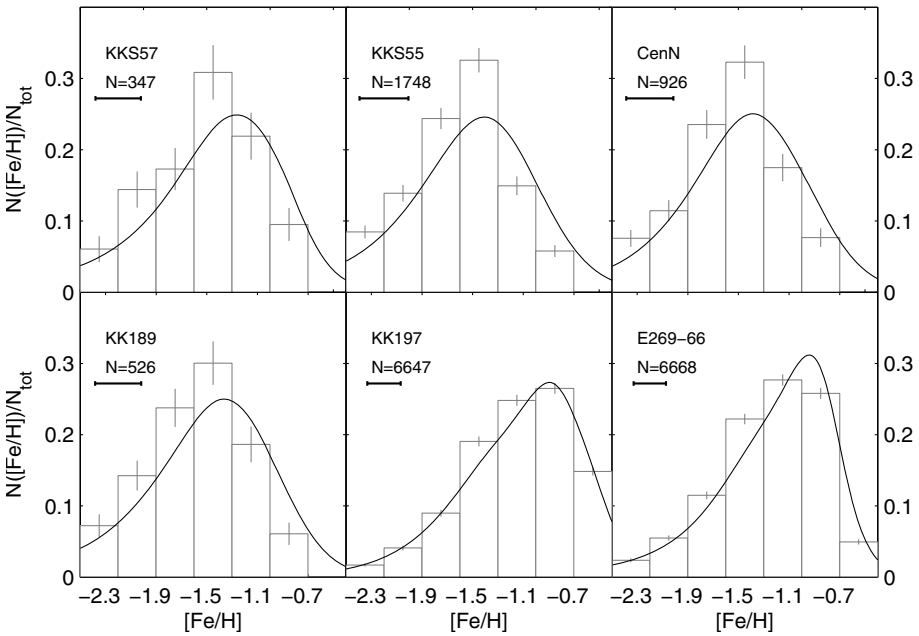

Fig. 3. Normalized metallicity distribution functions of the six dwarfs, derived via interpolation of isochrones at a fixed age (10 Gyr) and varying metallicity. Overlaid (black lines) are the MDFs convolved with the observational errors. Also plotted in the left upper corner is the median error on the individual values of [Fe/H], and the total number of stars considered (for details see Sect. 4).

most metal-poor isochrone and redder than the most metal-rich one), to avoid artificially metal-poor or -rich extremes in the results.

After deriving the metallicity values for each RGB star through interpolation, we show in Fig. 3 the metallicity distribution functions (MDFs) for our galaxies (each normalized to the total number of considered stars). The galaxies are again ordered by increasing absolute V magnitude. We chose not to correct the MDFs for completeness, since the latter changes very little within the magnitude range of the selection box. The errors in [Fe/H] we derived as follows: we performed 1000 Monte Carlo realizations of the interpolation process, varying the position of the stars on the CMD within their respective photometric errors (assuming Gaussian distributions), thus accounting for random errors. The median 1σ measurement errors of the individual values of [Fe/H] we plotted in the left corner of each subpanel. They range from ∼0.26 to ∼0.39 dex. The vertical (random) counting errors of each histogram bin we also take from the Monte Carlo realizations. Finally, in the figure we also draw the MDFs convolved with observational random errors (black lines). The effects of the systematic errors (on distance and reddening of the galaxy, taken from Karachentsev et al. 2007) on the MDFs are discussed in the next section.

All six galaxies contain populations that are on average metal-poor, with median values ranging from $\langle[\mathrm{Fe/H}]\rangle_{\mathrm{med}} = -1.56$ to -1.08 (the median value is more meaningful since the MDFs are not symmetric). There is no galaxy that appears to contain stars with a metallicity higher than [Fe/H] = −0.4. This result is influenced by our choice of the selection box, but for clarity in Fig. 1 we also overplot (for the galaxies KK197 and ESO269-66) an isochrone with [Fe/H] = −0.4; indeed, it can be seen how few stars lie redwards of this isochrone, so we conclude that our cutoff is reasonable. On the other side, the few stars that lie bluewards of the bluest isochrone (see Fig. 2) have probably been scattered there by photometric errors. Some may also be old AGB stars and some of them may be genuinely metal-poor RGB stars. We have no way of identifying the nature of such stars in our photometry. As stated earlier, we simply avoid extrapolating toward putative metallicities lower than covered by our isochrones.

The spreads in metallicity are quite broad. The nominal ranges of the metallicity covered in each galaxy are $\Delta[\mathrm{Fe/H}], obs \sim 2$ dex, and typically reach from [Fe/H] = −2.5 to values as high as [Fe/H] = −0.7 to −0.4. In the classical dwarf spheroidals in the Local Group, the full spectroscopically measured RGB metallicity range typically exceeds 1 dex (e.g., Grebel et al. 2003), so this wide range is in good agreement with what one might expect. When calculating a formal Gaussian dispersion, the metallicity spreads derived here are on the order of $\sigma[\mathrm{Fe/H}], obs \sim 0.4$–$0.5$ dex. This result requires some further attention. That is, we have to take the median error into account on the individual metallicity estimates, which comes from both photometric errors and from the close spacing of the isochrones on the CMDs. This simply means that the true metallicity dispersion is in fact narrower than derived. For a better estimate of the global intrinsic spread of the galaxy, $\sigma[\mathrm{Fe/H}], int$, we thus subtract in quadrature the median metallicity error from the observed dispersion. The final values range from $\sigma[\mathrm{Fe/H}], int \sim 0.10$ dex to ∼0.41 dex. This implies that the observed broadening of the RGBs is not only an effect of photometric errors.

In Table 2 we summarize the results as follows: Col. (1): name of the galaxy; (2): number of RGB stars for which we derive individual metallicity values; (3): percentage of Galactic foreground contaminants with respect to the number of stars in the selection box (see next section); (4): median [Fe/H] value computed from the MDF; (5): observed metallicity dispersion of the MDF (from Gaussian fit); and (6): intrinsic metallicity dispersion, after subtraction of the median measurement error.

The six histograms shown in Fig. 3 show a slow decline in the metal-poor direction, and a steeper slope on the metal-rich side. The results found here are similar to what has been observed in dwarf galaxies of the Local Group, both in terms of metallicity ranges and of MDF shape (e.g., Shetrone et al. 2001; Sarajedini et al. 2002; Tolstoy et al. 2004; Battaglia et al. 2006; Helmi et al. 2006; Koch et al. 2006; Bosler et al. 2007; Koch et al. 2007a,b; Gullieuszik et al. 2009). However, since in our work we are only able to present results based on limited assumptions because of the age-metallicity degeneracy, we do not compare the shapes of our MDFs to theoretical models or to Local Group members in more detail. We just note that

Table 2. Metallicity values derived for the studied sample of galaxies.

Galaxy	$N_{\rm RGB}$	$\%_{\rm cont}$	$\langle$[Fe/H]$\rangle_{\rm med}$	σ[Fe/H], *obs*	σ[Fe/H], *int*
KKs57	347	9	−1.45	0.46	0.28
KKs55	1748	2	−1.56	0.40	0.1
CenN	926	5	−1.49	0.40	0.15
KK189	526	5	−1.52	0.42	0.2
KK197	6647	1	−1.08	0.49	0.41
ESO269-66, KK190	6668	0.5	−1.21	0.42	0.33

the overall shapes of the MDFs resemble the MDFs of Galactic dwarf spheroidals, which suggests that similar evolutionary processes may have governed their star formation and enrichment histories.

5. Possible sources of error

The results presented in Table 2 will unavoidably be affected by the assumptions we made in the first place, i.e. a single old age, a negligible contribution to the MDFs by intermediate-age stars, and a scaled solar value for the α-element abundances. We now discuss the effects that these assumptions may have on the derived results in more detail.

5.1. Foreground contamination

For the HST/ACS data used here, we do not expect a high number of unresolved background galaxies in such a small field of view. In fact, they will be rejected by the DOLPHOT quality cuts, leaving a contamination of the CMDs of less than 3% (Dalcanton et al. 2009).

Regarding Galactic foreground contamination, we obtained estimates using the TRILEGAL models (Girardi et al. 2005). In the direction of the Centaurus A group and within the entire ACS field of view, there are on average ∼200 foreground stars expected. Additionally, the TRILEGAL models provide the photometry of the simulated stars, so that we are able to check which regions of the CMD would be most affected by foreground stars. In particular, we computed the percentage of contaminant stars found in the RGB selection boxes for each galaxy, after taking completeness effects into account (not all of the foreground stars would in fact be detected by the instrument), and we report the values in Table 2. They range from <1% to ∼9%, depending on the total number of stars in each galaxy.

In the upper panel of Fig. 4 we take the galaxy KK189 as an example. We plot a Hess density diagram of its stars on top of the CMD to illustrate its main features more clearly, and overplot the expected location of Galactic foreground stars derived from the TRILEGAL models. The predicted contaminants are few and are relatively uniformely distributed within the selection box, so we decided not to statistically subtract them from our RGB sample. Given the errorbars on the MDFs, the few stars that would be subtracted in such a procedure would indeed not change significantly our final results. With respect to the density maps presented in Sect. 6, the lowest contour level is always well above the value inferred for foreground contamination.

It could be argued that the Galactic models are not always able to reproduce the observed contamination perfectly. In particular, they underestimate the amount of objects with colors $V - I > 2$, partly because the contribution from thick disk and halo stars is uncertain at these colors and partly because there could be unresolved galaxies among them. However, the predicted star counts will differ in different color bins as a function

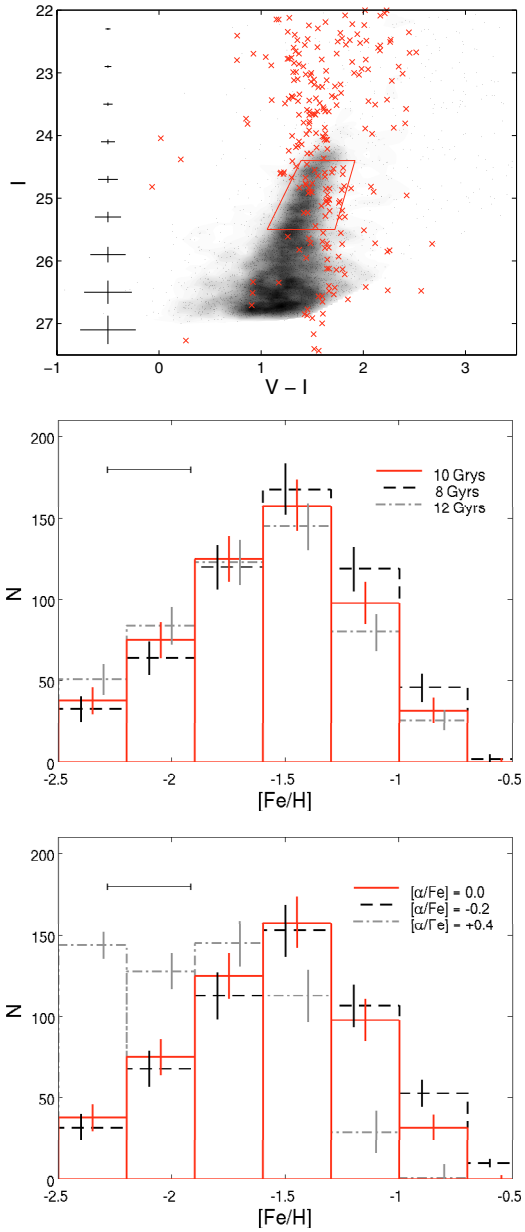

Fig. 4. *Upper panel.* Color–magnitude diagram of the dwarf spheroidal galaxy KK189, overlaid by a Hess density diagram of its stars. Shown also is the expected location of Galactic foreground stars (red crosses), estimated from the TRILEGAL models, and the selection box within which we derived metallicities. *Central panel.* Metallicity distribution function of KK189, derived via interpolation of isochrones at a fixed age and varying metallicity. The results are shown for 3 different ages (8, 10, and 12 Gry), and the errorbars are computed considering photometric errors. Also plotted in the left corner is the median individual metallicity error. *Lower panel.* As for the central panel, but keeping the age fixed at 10 Gyr and varying the α-enhancement abundance ([α/Fe] = −0.2, +0.0 and +0.4).

of the slope of the adopted Galactic IMF. Thus, the underestimation at red colors does not necessarily mean that the models are incorrectly reproducing the contamination at the position of our RGBs.

From Fig. 4 we also see that the contamination is higher in percentage for the upper part of the CMD above the TRGB, since the number of luminous AGB stars is very low. It is difficult from the optical observations alone to thus clearly distinguish between real AGB stars and foreground contaminants. This point will be considered again below, where we investigate the contribution from intermediate-age objects in more detail.

We also investigate the possible foreground contamination by projected halo stars of the dominant galaxy Centaurus A. This contamination may happen for the dwarfs that are found at very close projected distances from the giant elliptical, as in the case of KKS55 and KK197 (~48 and ~58 kpc, respectively). The RGB of Centaurus A has been investigated in detail in a series of papers (Harris et al. 1999; Harris & Harris 2000, 2002; Rejkuba et al. 2005) in order to derive the MDFs for fields at different galactocentric distances (8, 21, 31 and 38 kpc). If we assume that the halo of the giant elliptical extends further, out to the projected distances at which KKS55 and KK197 are found, and that the MDF shape of Centaurus A will not be very different from the more internal ones at these distances, we may then try to look for a possible contamination in the CMDs of our dwarfs. The photometric data collected for Centaurus A show a range in magnitude and color that is very similar to those of the dwarfs in our study. Thus, if the contamination from the Centaurus A halo stars is relevant, we should tentatively observe the RGB features of the giant elliptical even in our CMDs, i.e. we should see a very broad RGB with an extended metal-rich population (the peak metallicity for the outermost field of the galaxy is of [Fe/H] ~ −0.6). This is not found for the closest dwarf in projection, KKS55, which displays quite a narrow RGB, so we do not expect it to be true either for KK197. For the sake of completeness, we checked the radial distribution of the most metal-rich stars found in the CMD of KK197 and find them to be centrally concentrated, thus excluding a possible, diffuse contamination from the Centaurus A field.

5.2. Age assumption

In our metallicity derivation, we may be neglecting the stellar populations younger than the adopted age of 10 Gyr. In the CMDs of our targets (Fig. 1), some luminous AGB stars are indeed visible above the TRGB. The RGB could be contaminated by the stars coming from these intermediate-age populations that are on the RGB or ascending to the AGB phase, after having burned off the He in their cores. This contamination will be mostly in the metal-poor part of the derived MDFs, as relatively metal-poor, intermediate-age stars in their RGB/AGB stage would overlap the old, most metal-poor isochrones (age-metallicity degeneracy).

We give a rough estimate of the number of luminous AGB stars by considering Padova stellar evolutionary models (Marigo et al. 2008), since the Dartmouth isochrones do not model stages later than the RGB phase. We selected stars in a box that extends (in magnitude) from ~0.1 mag above the TRGB (this is greater than the photometric error in magnitude at these luminosities, so we made sure we are not picking RGB stars upscattered by photometric errors) up to ~1.1 mag above the TRGB. The range in color goes from the bluest edge of the RGB to $V - I \sim 3$. This selection criterion should still retain luminous AGB stars with ages from 1 to 10 Gyr, and with metallicities that are around the median metallicities derived for our galaxies (we assume that the intermediate-age populations will on average be slightly more enriched than the oldest and most metal-poor RGB stars).

We first compute the bolometric magnitudes for the candidate AGB stars with the empirical correction formula by Da Costa & Armandroff (1990) (for I-band magnitude). We then construct the bolometric luminosity function for the AGB stars, subtracting the number of predicted foreground stars for each magnitude bin. Since the star counts from the TRILEGAL models could be uncertain, we also try a second method, subtracting the number of stars that are found in a box with the same size of the AGB selection box, but just above it on the CMD. The two methods give results that are almost identical.

Having done this, we can now use the empirical relation derived in Rejkuba et al. (2006) (their Fig. 19), which connects the tip luminosity of the AGB and their age (for ages ≥1 Gyr). This method gives us a rough quantitative idea about the fraction of an intermediate-age population. Finally, we use an approximation for the formula of the fuel consumption theorem (Armandroff et al. 1993, originally from Renzini & Buzzoni 1986) to compute the expected number of luminous AGB stars per magnitude, given their fraction relative to the entire galaxy population. We then compare the results from our AGB counting to the predictions from this theorem, varying the fraction of the intermediate-age contaminants until the two values are similar.

With this method we obtain for each galaxy an estimate of the presence of stars with ages in the range ~4–8 Gyr. Younger stars are probably not present, as seen from our data, if we assume our foreground subtraction is correct. The results are as follows. For KK189, KKS57 and KK197, the estimated fraction of the intermediate-age population relative to the entire population is ~10%; ESO269-66 has a probable fraction of ~15%, while for KKS55 and CenN this number grows to ~20%. All of the stated fractions could possibly be lower limits to the true values, since the luminous AGB phase is short, so this stage could be poorly populated in the observed CMDs. These numbers are lower than what is observed in those few Local Group early-type dwarf galaxies with pronounced intermediate-age star formation (e.g., Leo I, Leo II, Fornax, Carina, NGC 147, and NGC 185, with fractions up to ~50%), but in line with previous studies of other early-type dwarfs in the Centaurus A group (Rejkuba et al. 2006).

At this point, in our MDFs we simply subtract the fraction of intermediate-age stars from the metallicity bins that are more metal-poor than the median metallicity. If we then recompute median metallicities and spreads for each galaxy, we find that for KK189, KKS57 and KK197, the median metallicities values would not change significantly since there are few intermediate-age stars, and the spreads would be slightly narrower (~5–10%); for ESO269-66 the new median metallicity is higher by ~5% and the spread is smaller by ~10%; finally, KKS55 and CenN would be only slightly more metal-rich (~2–3%), but the Gaussian metallicity spreads would practically go to zero.

However, we want to underline that the best way to look in more detail at luminous intermediate-age stars is instead to combine optical with near-infrared filters, because they are more luminous in the infrared and more easily separated from foreground contamination in the latter (e.g., Rejkuba et al. 2006; Boyer et al. 2009). We will consider ground-based (Very Large Telescope) images in J- and K-band in a companion paper (Crnojević et al. 2010, in prep.), in order to get better constraints on the epoch and strength of the more recent star formation episodes for our target galaxies.

The assumption of one single age for the galaxies' populations is also a strong simplification. To account for the spread in metallicity, extended star formation histories are needed. For early-type dwarf galaxies in the Local Group, complex star formation histories have been derived, and it was shown that no two dwarfs are alike, not even within the same morphological subtype (Grebel 1997). Although there are examples of Local Group dwarf spheroidals with predominantly old and metal-poor populations (e.g., Ursa Minor, Draco), the case of a single, ancient starburst is quite unlikely for most of them; on the contrary, large metallicity spreads have been detected, and the early star formation appears to have been low and continuous (e.g., Ikuta & Arimoto 2002; Grebel et al. 2003; Koch et al. 2006; Coleman & de Jong 2008; Koleva et al. 2009). Different models arrive at different durations to explain the observed metallicity spread (e.g., Ikuta & Arimoto 2002; Lanfranchi & Matteucci 2004; Marcolini et al. 2008). Assuming that the spread in metallicity is predominantly due to a spread in age, we repeated the metallicity interpolation process by choosing the three most metal-poor isochrones to have an age of 12 Gyr, and the most metal-rich ones an age of 8 Gyr. The result of this simple test is that, as one would expect, the peak of the MDF is less pronounced, and the intrinsic dispersion is slightly larger (∼15% in dex). However, since the observations are not deep enough to permit us to resolve the age-metallicity degeneracy from photometry of main sequence turnoff stars, a single age is the simplest assumption we can make without going into pure speculation. Moreover, as mentioned earlier, metallicity is the main contributor to the shape and width of the RGB; age has much less of an effect.

Having clarified this, our choice of setting the isochrone age to 10 Gyr is arbitrary, but as we can see from the central panel of Fig. 4, we may make such an assumption. We plot three different MDFs for KK189: one is derived from our chosen age, the other two are derived from ages slightly lower (8 Gyr) and slightly higher (12 Gyr) than the chosen one. It is clear that we do not introduce a significant bias when choosing one isochrone age over a slightly older or slightly younger one. Only in the case of an assumed younger age, there will be a higher number of metal-rich stars, but this will not significantly change the median metallicity value (the amount of change is ∼5% in dex) or the shape of the distribution. The reason for this relatively small dependence on age is that a decrease or an increase in age by a few Gyr has very little effect on the isochrones for these high ages. Hence a change in metallicity is much more noticeable, as it will have a stronger effect on the isochrones.

5.3. α-enhancement

For our adopted set of isochrones, we chose not to use α-enhanced tracks, because nothing is known about the level of the α-enhancements in our target galaxies. In the Local Group, the dwarf spheroidals present a broad range of [α/Fe] ratios at the metallicities of our galaxy sample (e.g., Shetrone et al. 2001, 2003; Sadakane et al. 2004; Geisler et al. 2007; Koch et al. 2008). In particular they can vary from sub- ([α/Fe] ~ -0.2) to super-solar ([α/Fe] $\sim +0.4$) values within the same dwarf, and the observed [α/Fe] ratios show a correlation with the [Fe/H] ratios, such that the α-element abundance tend to decrease for increasing [Fe/H] (e.g., Tolstoy et al. 2009; Koch 2009).

We again try the simple test described above for a choice of different ages, and let the α-element abundances vary for our isochrones. With a fixed age of 10 Gyrs, we compute the metallicities for isochrones again with [α/Fe] = −0.2, +0.2, and +0.4. The resulting MDFs are shown in the lower panel of Fig. 4 for [α/Fe] = −0.2, +0.0, and +0.4. Changing the α-element abundances by ±0.2 from the solar values gives a similar result as a change in age, such that lower (higher) α-element abundances would mimic a younger (older) set of isochrones, and the median metallicities would accordingly be higher (lower) by less than ∼5%. When choosing [α/Fe] = +0.4, the median metallicity is lower by ∼30%, and the metallicity spread is almost doubled. However, this is a rather extreme assumption, since the most probable case is the one where we have a spread of α-enhancement values. This could again be included in our computation by choosing the most metal-poor and oldest isochrones to have subsolar α-enhancement, and the most metal-rich and youngest to have super-solar α-enhancement. Our simple test is primarily intended to explore the parameter range. It demonstrates that the resulting median metallicities would be slightly lower (∼15% in dex), while the metallicity spread would be much greater (3–4 times) when a range of [α/Fe] values is considered.

5.4. Systematic errors

In our analysis, we adopt the values for distance and foreground reddening from Karachentsev et al. (2007) and from the Schlegel extinction maps (Schlegel et al. 1998), respectively. These are affected by uncertainties of ∼7% and ∼10% of the values listed in Table 1. If we let one of these two parameters vary within its errorbars, the isochrones overplotted on the observed CMDs will all be shifted by the same amount.

We first test how the derived median metallicities and the metallicity spreads change if we change the adopted distance value within its errorbars. We find that for distances higher (lower) than the adopted one, the median metallicities are lower (higher) by ∼10% (meaning ∼0.10–0.15 dex), while the spreads are also higher (lower) by ∼20%. Similarly, for higher (lower) foreground reddening values the resulting median metallicities will be higher (lower) by ∼3% and the spreads lower (higher) by ∼10%.

5.5. Stellar evolutionary models

As a test, we also repeated our entire analysis using Padova isochrones (Marigo et al. 2008), with an identical age and metallicity grid. The results are quite similar overall, from the shape of the MDFs to the presence of metallicity gradients and distinct stellar populations (see next section), but the average metallicities found for each galaxy are systematically higher by ∼0.3 dex on average. However, a detailed comparison between different theoretical models goes beyond the goals of our work (for some examples, see Gallart et al. 2005; Glatt et al. 2008a,b; Goudfrooij et al. 2009; Sarajedini et al. 2009).

6. Metallicity and population gradients

We now look for metallicity gradients within the galaxies and for projected spatial variations in their stellar populations.

6.1. Metallicity gradients?

To take into account that the galaxies do not have a perfectly circular shape, we consider elliptical radii from now on. The determination of the ellipticity for each galaxy follows the method of McLaughlin et al. (1994). In Fig. 5 we show the individual metallicity values for the RGB stars as a function of elliptical

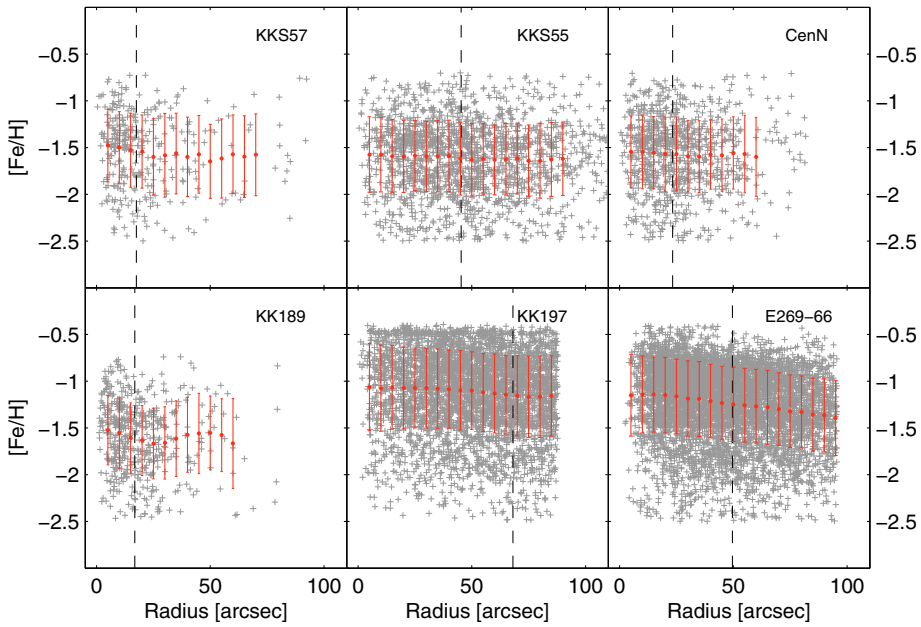

Fig. 5. Metallicities of individual RGB stars as a function of elliptical radius for the six galaxies. The projected half-light radius r_h is plotted as a dotted line in each subpanel. A running mean (red points) is also drawn for each galaxy.

radius. We plot the data until the last ellipse that is entirely contained within the ACS field of view, because data beyond that point are incomplete in metallicity. That is, we could correct the number of stars to account for not observing the entire area of the ellipse, but we could not have any metallicity information about the stars that lie outside the instrumental field of view. For the galaxies KKs55, KK197, and ESO269-66, the instrumental field of view does not cover their whole extent. We also overplot the projected half-light radius for each galaxy, derived as described below.

We compute projected, completeness corrected surface density profiles from our RGB stars, and fit them with 3-parameter King models (King 1962). However, these models only yield poor results when we attempt to simultaneously fit both the very central parts and the outskirts of the dwarf galaxies. We thus also derive I-band surface brightness profiles from star counts, and fit them with Sersic profiles (Sersic 1968). This is a generalized exponential function of the form $I(r) \sim I(r_h)\exp[-(r/r_h)^{1/n}]$, where the surface brightness is expressed in terms of intensity. It should be noted that some authors use the index n instead of $1/n$ for this type of parametrization. The free parameters for the Sersic profile are the effective (half-light) radius r_h, a shape parameter n that characterizes the curvature of the profile and the surface brightness at the radius r_h. The values derived here are reported in Table 3. We cannot make direct comparisons with the values previously published for our sample of galaxies because such studies consider surface brightness profiles from different bands (Jerjen et al. 2000a) or perform the fit with a simple exponential profile (Sharina et al. 2008). The results derived in this work are nevertheless consistent with the ones found in the aforementioned studies. For the sake of clarity, we have to underline that we construct our surface density profiles as a function of elliptical radius. However, other authors often define a "reduced radius" ($r_{red} = \sqrt{ab}$, with a and b as the semi-major and semi-minor axes, respectively) to account for the ellipticity of the galaxy. For a small ellipticity, the two radii are consistent with each other, but in the case of a high ellipticity, they can differ substantially. In our sample, the galaxy KK197 is very elongated so its "reduced" half-light radius would result in a lower value than the one computed from our profiles. For completeness, we apply the correction for ellipticity to our derived half-light radii and also report them in Table 3 ($r_{h,red}$). We also use this information later, when looking for different stellar populations within our galaxies.

Table 3. Parameters from Sersic profiles.

Galaxy	r_h [a]	$r_{h,red}$ [b]	n
KKs57	17.5 ± 0.8	14.2 ± 0.6	0.97 ± 0.14
KKs55	45.3 ± 0.6	43.9 ± 0.6	0.79 ± 0.04
CenN	23.3 ± 0.6	22.5 ± 0.5	0.73 ± 0.05
KK189	16.8 ± 0.5	14.9 ± 0.4	0.88 ± 0.06
KK197	68.1 ± 1.5	47.2 ± 1.0	0.60 ± 0.05
ESO269-66, KK190	49.6 ± 0.6	43.6 ± 0.5	0.76 ± 0.04

Notes. [(a)] Computed from surface brightness as a function of elliptical radius. [(b)] Computed from surface brightness as a function of "reduced" radius $r_{red} = \sqrt{ab}$ (see text for details).

Coming back to Fig. 5, it is not easy to see a possible trend in these plots, so we also compute and plot a running mean for each galaxy (in steps of ~5 arcsec). Simple linear fits reveal flat or weak overall gradients. For KKS55, KK197, and ESO269-66, the results are ~–0.043, −0.09, and −0.17 dex per arcmin, respectively (or ~–0.036, −0.075 and −0.15 dex per kpc). For the three remaining galaxies, which are less extended than the ones above, a weak gradient is observed in the central regions, while in the outer parts it tends to flatten (and the statistics tend to worsen because of the small number of stars in the outskirts). We find that: for KKS57, within the inner ~40 arcsec, we have a gradient of ~–0.18 dex per arcmin (~–0.15 dex per kpc); for CenN, the value is of ~–0.078 dex per arcmin (~–0.065 dex per kpc) in the inner ~40 arcsec; for KK189, within the inner ~30 arcsec, the linear fit gives ~–0.36 dex per arcmin (~–0.3 dex per kpc). Due to the large errorbars reported in Fig. 5, we may conclude that an *overall* metallicity gradient is definitely present for ESO269-66, while KKS57 and KK189 only show hints of a gradient in their central regions. Finally, for ESO269-66 we have no information about the stellar population of its nucleus, because it is not resolved in the photometry.

We may further want to check that there are differences in the stellar population of the galaxies, as observed in some early-type dwarfs in the Local Group. For each galaxy we thus divide

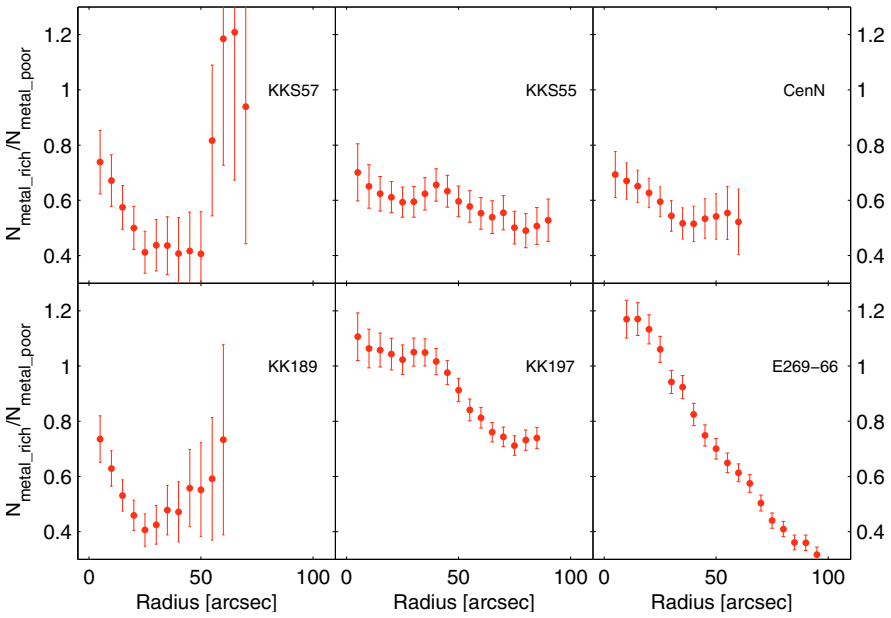

Fig. 6. Ratio of metal-rich to metal-poor stars as a function of elliptical radius. These stars have metallicity values $>(\langle[\mathrm{Fe/H}]\rangle_{\mathrm{med}} + 0.2)$ and $<(\langle[\mathrm{Fe/H}]\rangle_{\mathrm{med}} - 0.2)$, respectively.

the stars with derived metallicities in two subsamples. The first (*metal-poor*) subsample contains stars with metallicity values $<(\langle[\mathrm{Fe/H}]\rangle_{\mathrm{med}} - 0.2)$, while the second (*metal-rich*) subsample has values $>(\langle[\mathrm{Fe/H}]\rangle_{\mathrm{med}} + 0.2)$. We thus avoid any significant overlap for the subsamples, by excluding the values around the peak of the metallicity distribution functions.

First of all, we check the results derived for the metallicity gradients by plotting the ratio of metal-rich to metal-poor stars as a function of elliptical radius (Fig. 6, where the errorbars come from the Monte Carlo realizations described above). The ratio is decreasing overall with radius for all of the galaxies. For KKS57, CenN, and KK189, this is valid out to a bit more than the r_{h}, after which the ratio tends to be dominated by statistical errors and fluctuations. These stem from small-number statistics and our averaging over an elliptical radius, thus not taking asymmetric features into account. For the three other galaxies, the ratio decreases over their whole extent.

6.2. Population gradients?

For the two metallicity subsamples, we then derive I-band surface brightness profiles from star counts (corrected for radial incompleteness) and plot them in Fig. 7 (normalized to the total number of considered stars). Indeed, for KK197 and ESO269-66 we clearly see a difference between the two subpopulations. To quantitatively test whether the two subpopulations are truly separated, we performed two-sided Kolmogorov-Smirnov (KS) tests, again varying the metallicity of each star within its metallicity error. In this way we could assess the robustness of our results. The values derived from the KS tests are reported along the surface brightness profiles in Fig. 7: for KKS57, CenN, and KKS55, there is a probability of ∼40% (i.e., less than 1σ significance level) that the two subsamples come from the same parent distribution; for KK189, this probability goes down to ∼10% ($\sim 2\sigma$); finally, for KK197, and ESO269-66 the null hypotesis can be rejected (with a probability of, respectively, 0.15% and $\ll$0.01%), thus these galaxies do show significantly separated subpopulations. This is a robust result, even though our subdivision into subsamples is arbitrary and the radial distribution of the subsamples partly overlaps, but with these data we have no way of investigating whether *more* than two stellar subpopulations are present.

Jerjen et al. (2000a) performed surface photometry in the B and R-bands of dwarfs in the Centaurus A and Sculptor groups. Their sample contains three of our galaxies (KK189, KK197, and ESO269-66). Jerjen et al. (2000a) had a slightly larger field of view for their observations than provided by our ACS data, but the results are consistent with ours. It is particularly interesting to look at their $B - R$ color profiles as a function of radius: for KK189 the color profile stays constant, while for the other two dwarfs in common with our study, they become redder for radial distances from the center greater than the projected half-light radius. This supports our results regarding an older/more metal-poor population that dominates the outskirts of these galaxies.

We can also divide the stars into two subsamples depending on their distance from the galaxy center, e.g., $r < r_{\mathrm{h}}$ and $r_{\mathrm{h}} < r < 2r_{\mathrm{h}}$. This is done to compare the results for each galaxy with a fixed physical quantity, the half-light radius, and in order to do these comparisons in the future in other studies. We chose the ranges such that there are enough stars in each sample. The ACS data cover (at least) $2r_{\mathrm{h}}$ for (almost) all of our target galaxies. The only exception is KK197, for which the data cover less than $2r_{\mathrm{h}}$, so that the stars in the second subsample have distances ranging from r_{h} up to $\sim 1.35r_{\mathrm{h}}$. We check for the less extended galaxies whether the results change significantly when choosing a larger second interval ($r_{\mathrm{h}} < r < 3r_{\mathrm{h}}$), but we do not see any evidence of that. We then derive normalized (to the total number of considered stars) MDFs for the two radius-selected subsamples. For the galaxies with no significant signature for two different subpopulations, the normalized MDFs are indistinguishable within the errorbars, but they show a marked difference as expected for KK197 and ESO269-66. We report the normalized MDFs for the last two dwarfs in Fig. 8. That the data do not cover the full extent of KK197 within $2r_{\mathrm{h}}$ does not change our conclusions, since a gradient is already clear in the inner regions of the galaxy. KK197 and ESO269-66 are classified as dwarf ellipticals, they are the most luminous galaxies in our sample, and they are located very close to the central dominant galaxy of the group (see Fig. 11).

However, in these kinds of analyses one has to keep two aspects in mind. First, by looking at properties as a function of projected radius, possible non-radial gradients can be averaged

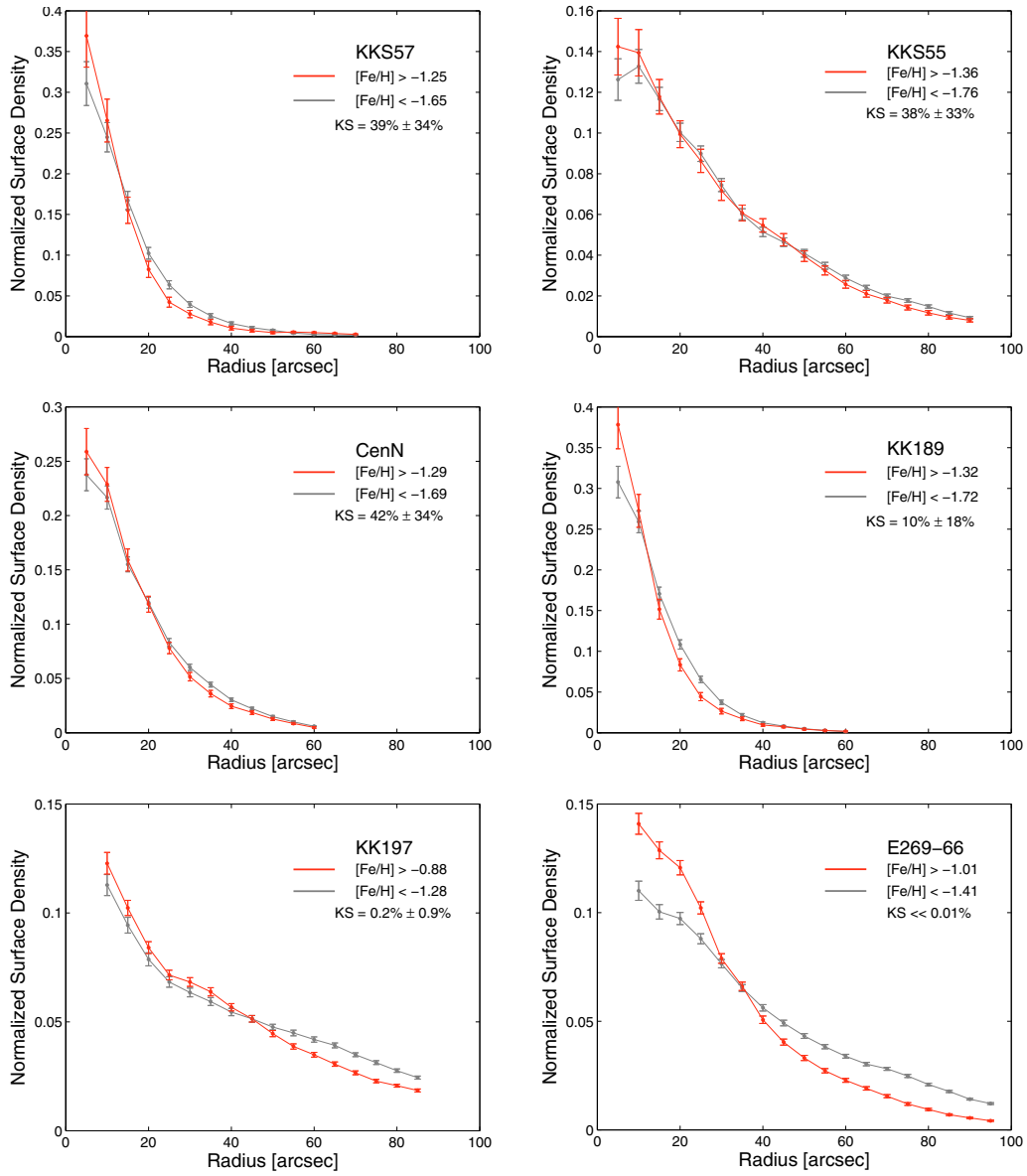

Fig. 7. Normalized surface brightness profiles as a function of elliptical radius. For each galaxy there is a distinction between *metal-poor* (solid gray lines) and *metal-rich* (solid red lines) stars (with metallicity values $<(\langle[Fe/H]\rangle_{med} - 0.2)$ and $>(\langle[Fe/H]\rangle_{med} + 0.2)$, respectively). We also report the result of a KS test on the cumulative distribution functions of the two subsamples, in order to statistically assess whether they belong to the same parent population or not (see text for details).

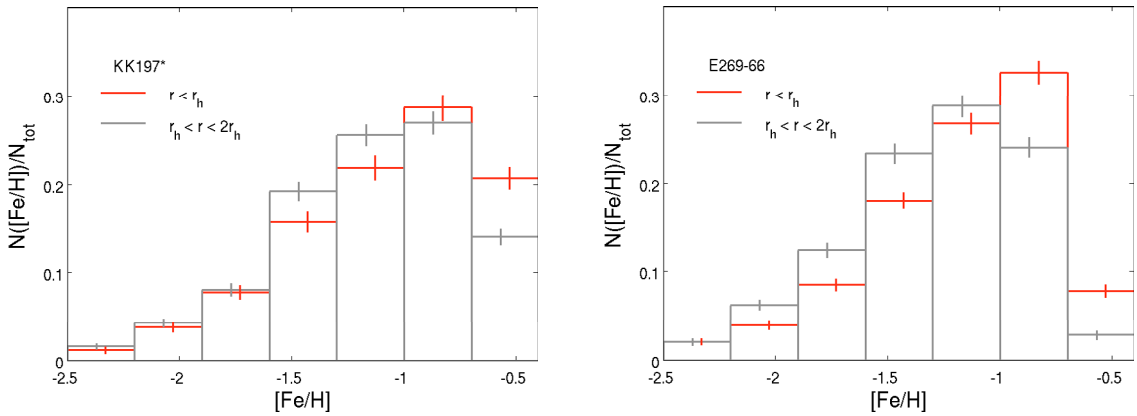

Fig. 8. Normalized metallicity distribution functions for the inner and outer regions of KK197 and E269-66. The RGB stars are divided into two subsamples, respectively with distances of $r < r_h$ and $r_h < r < 2r_h$ from the galaxy center. For KK197 the data do not go out to $2r_h$, so the second subsample contains stars with distances that go from $r > r_h$ until the borders of the CDD frame (corresponding to $\sim 1.35 r_h$).

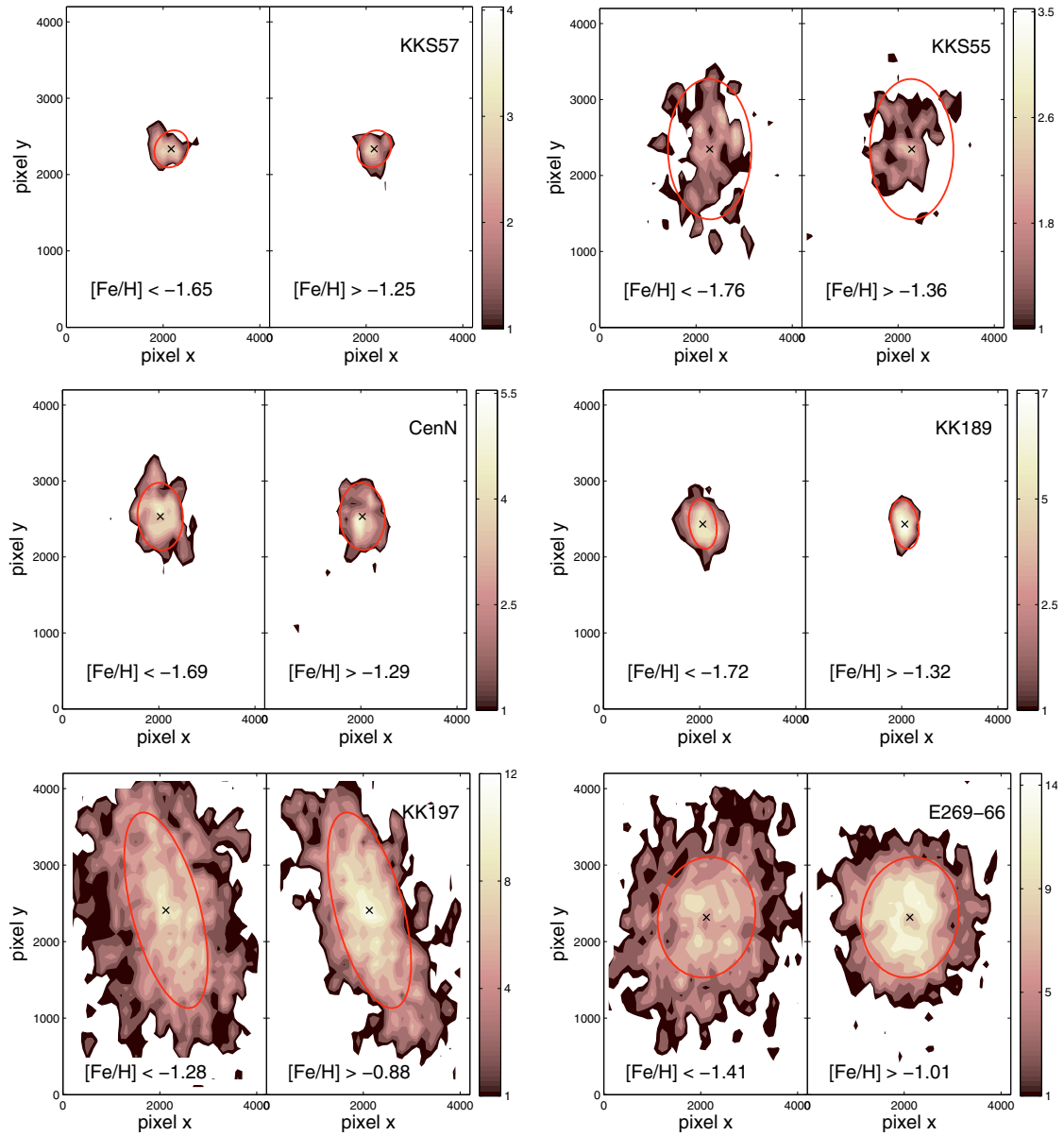

Fig. 9. Density maps for the galaxies, each divided into two subsamples. For each galaxy, the *left* (*right*) *panel* shows *metal-poor* (*metal-rich*) stars with metallicity values $<(\langle[Fe/H]\rangle_{med} - 0.2)$ $(>(\langle[Fe/H]\rangle_{med} + 0.2))$. The color scale is the same for the two subsamples, normalized to the peak density value of the *metal-rich* one, and the density values are listed in units of number of stars per 0.01 kpc^2. Ten equally spaced isodensity contours are drawn starting at the 1σ up to the 3σ significance level (4σ for KK197 and ESO269-66). The center of each galaxy is indicated with a black cross, and its half-light radius with a red ellipse (see Sect. 6 for details).

out. We thus also compute area density maps for the two subsamples in the following way. At the mean distance of the group (∼3.8 Mpc), 1 arcsec approximately corresponds to ∼0.02 kpc. We first count the number of neighbors within ∼0.03 kpc^2. This value is chosen to avoid introducing any small-scale noise or artificial substructures, but to permit us to still recognize overall features. Then we convolve the results with a square grid and get a final resolution of 0.01 kpc^2. The resulting density maps are shown in Fig. 9. The color scale is the same for both subsamples of each galaxy, normalized to the peak density value of the *metal-rich* sample, and the values are reported in units of number of stars per 0.01 kpc^2. We draw 10 equally spaced isodensity contour levels starting at the 1σ significance level up to the 3σ significance level (4σ for KK197 and ESO269-66). In every case, the outer contours have values of many (∼5 on average) σ above the Galactic foreground level.

The density maps of the two subsamples in each galaxy do not show striking differences. In each case, the subsamples' distributions follow the elongation of the galaxy. However, we can see that the *metal-rich* stars tend to be more centrally concentrated than the *metal-poor* ones in KK197 and ESO269-66. There are some fluctuations and asymmetries within the galaxies, to some extent caused by small-scale substructure and poor sampling in the outskirts. In the most massive galaxies, the ACS gap between its two CCDs is visible in the density maps (a horizontal line at pixel $y \sim 2000$), but this does not affect their general features. For KK197, an unresolved globular cluster is found near the position of the central peak (Georgiev et al. 2008), which may in fact represent a nucleus. For the nucleated galaxy ESO269-66, a depression in the density map is seen at the center, because we chose to leave out the nucleus because of the high crowding in that region.

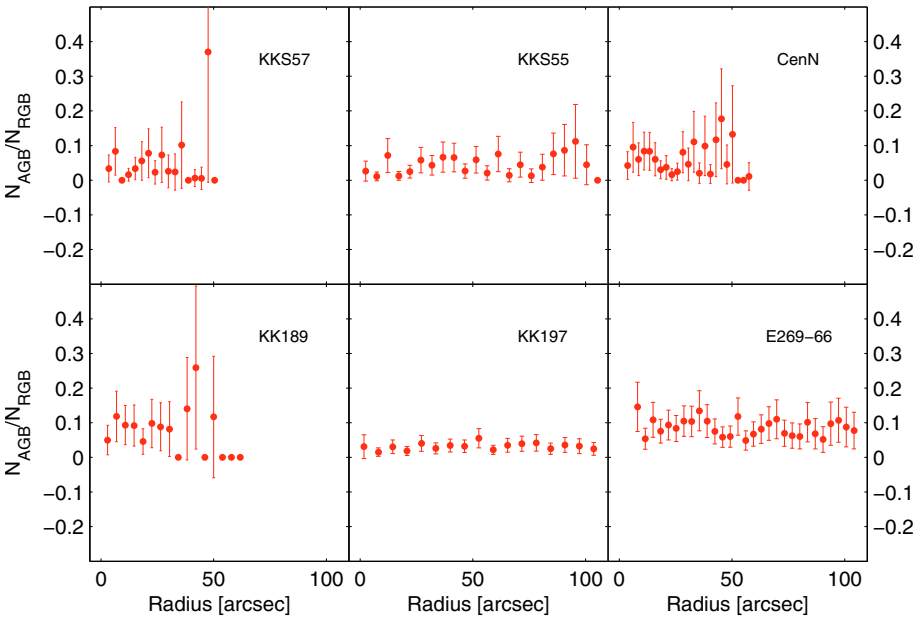

Fig. 10. Ratio of luminous AGB to RGB stars as a function of elliptical radius (see text for details on the selection of the two subsamples).

The second thing that has to be mentioned is that, as seen in the previous section, there is a non negligible intermediate-age population for some of our galaxies. The intermediate-age stars could, in principle, bias the derived metallicity gradients. We thus have a qualitative look at the radial distribution of the luminous AGB stars. We computed the number of AGB and RGB stars (selected as described in Sect. 4) in elliptical annuli of ∼4 arcsec width. We corrected the counts for radial incompleteness and also subtracted the estimated number of contaminants for AGB and RGB separately. This has to be done because the amount of relative contamination is very different for the two samples because of having fewer luminous AGB stars than RGB stars. We then computed the ratio between AGB and RGB stars and considered it to be a function of radius. The results are plotted in Fig. 10. The strong fluctuations in these plots are just reflecting the poor statistics. In almost every case, this ratio stays nearly constant over the full extent of the galaxy. Only for ESO269-66 do the inner ∼20 arcsec show a slightly higher AGB to RGB ratio, revealing a small amount of intermediate-age AGB stars concentrated in the inner region of this galaxy. As discussed before, this younger population would – at least qualitatively – increase the number of apparently blue, metal-poor RGB stars, thus biasing the metal-poor subsample. Nonetheless, we see that the more metal-rich stars are clearly more centrally concentrated (Figs. 7 and 8). On the other hand, the metallicity gradient that we find for this galaxy is still significant, and it could be even more pronounced if some of the central stars that we identify as metal-poor RGB stars were in fact more metal-rich, low-luminosity AGB stars superimposed on the RGB.

7. Discussion

To illustrate where the target galaxies are located within the Centaurus A group, we plot the position in the sky of the galaxies in this group in Fig. 11, using the data from Karachentsev et al. (2007). The upper panel shows the distribution of dwarfs with positive tidal index (i.e., belonging to the group) around the two giant galaxies Centaurus A and M 83, which form two distinct subgroups. In the lower panel of the figure, we zoom in around Centaurus A, since all of the galaxies studied here belong to the Centaurus A subgroup. This is obviously quite a dense region,

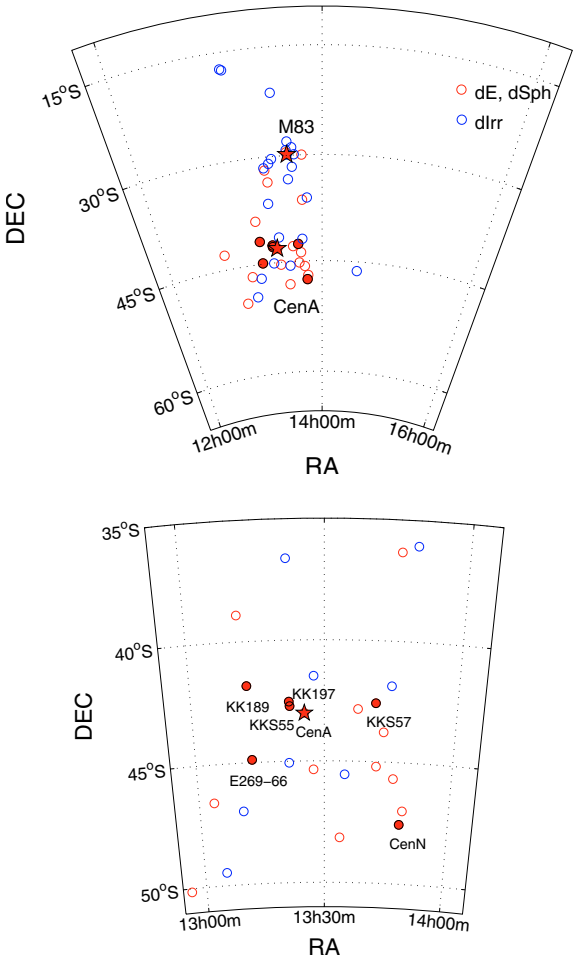

Fig. 11. *Upper panel.* Positions in the sky of the galaxies belonging to the Centaurus A group (from Karachentsev et al. 2007). Red symbols indicate early-type dwarfs (dE and dSph), while blue symbols are for late-type dwarfs (dIrr). Two red stars are drawn at the positions of the two dominant giant galaxies Centaurus A and M 83, around which the smaller companions cluster and form two distinct subgroups. The filled circles represent the dwarfs studied here. *Lower panel.* Same as above, just zoomed in a smaller region around Centaurus A, where the galaxies studied here are located (as labeled in the plot).

because it contains approximately the same number of galaxies within a fixed radius as our Local Group, with the difference that the census for Centaurus A is likely to be incomplete (e.g., Jerjen et al. 2000a; Rejkuba et al. 2006).

The six early-type dwarfs of our sample have quite a wide range of luminosities (see Table 1), and their morphological types vary from dwarf spheroidals (KKs57, KKs55, CenN, and KK189) to dwarf ellipticals (KK197 and ESO269-66, the latter being a nucleated galaxy). What they have in common is the absence of any recent star formation (as traced by Hα, or young populations from CMD), and there is no significant amount of HI detected that would allow for ongoing or future star formation. For example, Bouchard et al. (2007) investigated the gas content in three of our target dwarfs (KK189, KK197 and ESO269-66) and find only upper limits for their HI masses (<1.6, <2.9 and $<1.0\times10^5$ $M_\odot$). Moreover, only upper limits can be found for the star formation derived from Hα emission: for KK189, KK197, and ESO269-66 the values reported by Bouchard et al. (2009) are $<0.4\times10^{-5}$ $M_\odot$ yr^{-1}.

The metallicities derived here can be compared to the work of Sharina et al. (2008). These authors derive the mean metallicities for a large sample of nearby dwarfs, among which there are also our target objects. Sharina et al. (2008) apply the empirical formula $[Fe/H] = -12.64 + 12.6(V-I)_{-3.5} - 3.3(V-I)^2_{-3.5}$ (Lee et al. 1993), which infers the mean metallicity from the mean color of the RGB at an absolute magnitude of $M_I = -3.5$. Their derived values are all slightly lower (~10–15% in dex) than the values found with our isochrone interpolation method, but still consistent within the errors, if we consider the difference (~0.1 dex) between the empirical metallicity scale from the above-mentioned formula and the one used in the Dartmouth isochrone models. This discrepancy is also possibly due to a different selection of stars for the computation of the mean color of the RGB.

Sharina et al. (2008) further plot the color spread as a function of luminosity and suggest that the linear correlation between these two quantities could stem from a more intense star formation in more massive galaxies, probably because of denser gas reservoirs. They do, however, note a very high *color* spread for the galaxy KK197, twice what could be expected for its luminosity. Sharina et al. (2008) suggest this is the consequence of a possible strong mass loss. If we plot our derived *metallicity* spreads as a function of luminosity, KK197 indeed appears to be slightly displaced from the linear relation shown by the other galaxies, and so does also KKS57. Looking at the position of these two galaxies within the group (Fig. 11), and also their deprojected distance from Centaurus A (see below), they are located not far from the giant elliptical, but we have no way of adding more information about possible environmental effects because nothing can be said about the orbits that the dwarfs had in the past. However, Bouchard et al. (2007) point out that KK197 and ESO269-66 could both be influenced by the close radio lobes of Centaurus A, through which they may pass during their orbits and which may have contributed to the removal of the neutral gas content. In fact, ESO269-66 appears to have a particularly low HI gas mass to visual luminosity ratio, suggesting that some external agent could have contributed to the loss of its gas content. Although KKS55 is (in deprojection) located very close to Centaurus A as well, it does seem to contain a slightly greater fraction of intermediate-age stars, as compared to KKS57, KK197 and ESO269-66. This could possibly imply that this galaxy may now be on its first close approach to Centaurus A.

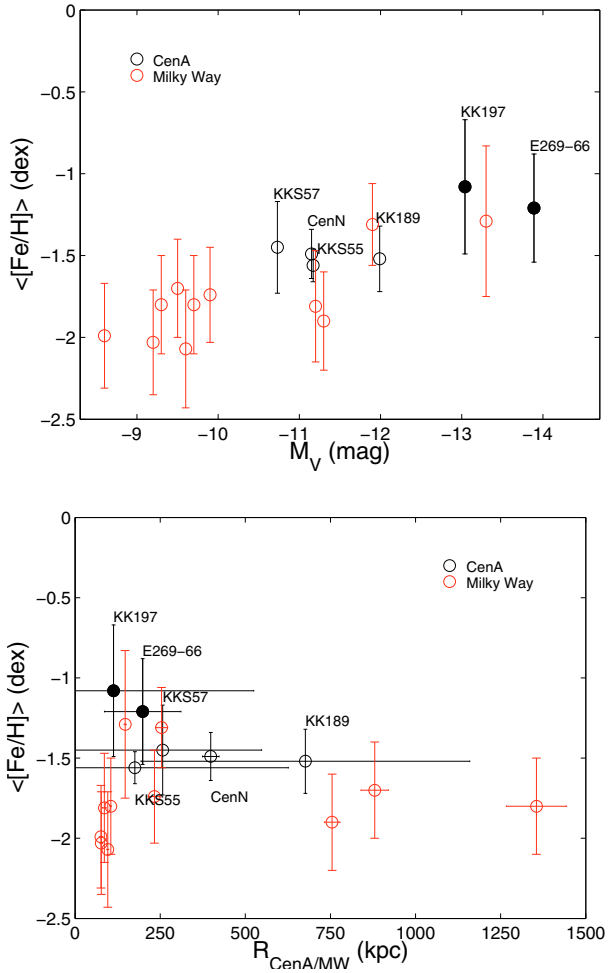

Fig. 12. Median metallicity plotted as a function of (*upper panel*) absolute V luminosity and (*lower panel*) deprojected distance from the dominant group galaxy. The black symbols represent the Centaurus A group dwarfs studied here (filled circles are dwarf ellipticals, the others dwarf spheroidals), while red symbols are for Milky Way companions.

Given the restricted amount of information we can derive from the data considered here, it is difficult to make a detailed comparison to the dwarf galaxies of our own Local Group. However, there are some points that suggest that the smallest objects in these two groups may have had a similar history. Like the complex and different star formation histories seen in our neighborhood, we see that the metallicity and stellar population properties in our target dwarfs differ from each other (e.g., median metallicity, metallicity spread, fraction of intermediate-age stars). However, it looks like there are no purely old dwarfs in our sample such as Ursa Minor or Draco in the Local Group.

In our results, all of the studied dwarfs are relatively metal-poor, as is expected for galaxies with such low luminosities. For comparison, dwarf spheroidals in the Local Group that lie in the same range of luminosities have mean values of [Fe/H] = −1.7 to −1.2 (see, e.g., Mateo 1998; Grebel et al. 2003; Koch 2009), hence on average slightly more metal-poor than our sample (see Fig. 12). This small difference could come from the measurement techniques, on one hand detailed spectroscopy and on the other photometry. Moreover, as mentioned in Sect. 4, the metallicities derived here could possibly be upper limits because of our assumptions about age and α-enhancement, so we conclude that on average there are no significant differences between the dwarfs of the two groups. Dwarf galaxies with even

lower luminosities have recently been found in the Local Group, which have even lower metallicities, but these objects are intrinsically too faint to be observed in the existing surveys at the Centaurus A group distance. This naturally leads us to the metallicity-luminosity relation, already analyzed in detail for the Local Group and other environments by many authors (e.g. Mateo 1998; Grebel et al. 2003; Thomas et al. 2003; Lee et al. 2007; Sharina et al. 2008). The six galaxies analyzed here have already been included in the metallicity-luminosity relation of Sharina et al. (2008, Fig. 9). They show that this relation is very similar for the dwarfs in the Local Group and those in other groups and in the field within a distance of ∼10 Mpc. They also comment on a few early-type dwarfs that show lower metallicities than all of the others, pointing out that they resemble dwarf irregulars in their metallicity content and could thus be in a transition phase. Among the galaxies with metallicity values lower than expected, there are the three galaxies in common with our study (KKs55, CenN, and KK189). In the upper panel of Fig. 12, we again plot the metallicity-luminosity relation with the small sample of values derived in our study and adding the values for dwarf spheroidals that are companions to the Milky Way (taken from the literature compilation by Kalirai et al. 2010). There does not seem to be any major displacement of our target dwarfs from a linear relation that represents Local Group dwarfs. This relation will, however, be considered again with the addition of data for late-type dwarfs of the Centaurus A group in two forthcoming papers (Crnojević et al. in prep.).

The other panel in Fig. 12 represents the dependence of metallicity on the deprojected distance from Centaurus A, and the same is reported also for Milky Way dwarf spheroidals. We compute the distances from the host galaxy by considering the radial distances listed in Karachentsev et al. (2007) and the angular ones derived by Karachentsev et al. (2002). In this relation, our dwarf spheroidals seem to resemble what is seen for Milky Way companions: neither the Centaurus A nor the Milky Way companions show any obvious trend with galactocentric distance from their massive primary (other than increased scatter in close proximity to a massive galaxy). The two dwarf ellipticals KK197 and ESO269-66 are slightly more metal-rich, similar to the dwarf elliptical companions of M 31. There are no such objects in the vicinity of the Milky Way. Finally, we also look for a possible correlation of the metallicity with the tidal index (i.e., a measure of the degree of isolation of a galaxy, with higher values corresponding to denser environments, Karachentsev et al. 2004), but find no trend.

The last aspect investigated in our study is the possible presence of subpopulations with a different metallicity content. For the Local Group, photometric, detailed spectroscopic, and in some cases also kinematic studies revealed dwarfs with distinct subpopulations, but also dwarfs that do not present any such trend, and only weak metallicity gradients. It it thus not surprising to also find such diversity also in the Centaurus A group. Recent simulations by Marcolini et al. (2008) provide a convincing model for the formation of population gradients and can even account for the formation of subpopulations distinct in metallicity and kinematics. According to this model, population gradients are the natural consequence of "the chemical homogeinization of the interstellar matter, together with the combined inhomogeneous pollution by supernovae type Ia", provided that star formation lasts for several Gyr. In our sample we have two cases (KK197 and ESO269-66) where the metallicities are quite high and where moderate metallicity gradients are found. Defining a metal-poor and a metal-rich subsample of stars, we do find evidence of at least two subpopulations with different radial distributions, even though our separation between the subsamples is arbitrary. This could be the effect of a low, extended star formation at the early stages of these galaxies' lives, which would enrich the subsequent stellar populations. Since these are the two most luminous galaxies, the retention of some neutral gas due to deeper potential wells could in principle help keep the star formation active for some Gyr. The possible existence of small age gradients in old populations with ages >10 Gyr cannot be resolved in our data, since the effect of age on the isochrones is too small and we have no other way to disentangle age and metallicity on the upper RGB, but it is almost certainly present and could explain the observed metallicity spreads and gradients.

8. Conclusions

We have analyzed stellar point-source photometry for six early-type dwarf galaxies in the Centaurus A group (at an average distance of ∼3.8 Mpc), using archival HST/ACS data. Their color–magnitude diagrams show broad RGBs without any evidence of young (<1 Gyr) populations, so we assume a predominantly old age for their stellar content. We note, however, that our target galaxies also exhibit a small number of luminous AGB stars above the tip of their RGBs, indicative of some contamination with intermediate-age stars (in the range ∼4–8 Gyr). To derive photometric metallicities for the luminous red giants in our sample, we chose Dartmouth isochrones (Dotter et al. 2008), since they have been shown to provide an excellent fit to the full extent of color–magnitude diagrams of both old and intermediate-age star clusters. Fixing the age of the isochrones at 10 Gyr and assuming a solar scaled α-element abundance, we let the metallicity vary and interpolate between the isochrones to get individual metallicity values for stars on the RGB. The results show in all the cases: 1. an on average *metal-poor stellar content* ($\langle$[Fe/H]$\rangle$ = −1.56 to −1.08), and 2. a *spread of metallicities* (internal dispersion of 0.10–0.41 dex). We further estimate the amount of bias in our results due to the presence of intermediate-age stars (which account for ∼10 to ∼20% of the entire population), and find that the metallicity spreads are likely to be the result of this contamination for two of the target galaxies. For the other objects, we show that the presence of extended early-star formation episodes (which are indeed very likely) and of a range of α-element abundances would eventually broaden the derived metallicity spreads, and make the median metallicities lower by ∼15%.

We investigate the possibility of metallicity gradients as a function of elliptical galactic radius. We find a moderate overall gradient for one dwarf elliptical (−0.17 dex per arcmin, or −0.15 dex per kpc), and hints of a gradient in the inner regions of two dwarf spheroidals. We further investigate possible differences in the stellar spatial distributions, splitting the stellar content of each galaxy into metal-poor and metal-rich stars. For the two dwarf ellipticals, which are also the most luminous galaxies of our sample, we can reject the null hypotesis that the two subpopulations come from the same parent distribution with a high statistical confidence level, with the more metal-rich stars being more centrally concentrated.

A detailed comparison to well-studied dwarfs in the Local Group is not possible because of the intrinsic uncertainties of our methods. However, the results derived in this study (metal-poor stellar contents, broad metallicity spreads, metallicity gradients) are overall very similar to what is found for the early-type dwarfs in our Local Group, even though the Centaurus A group is a denser environment, possibly in a more evolved dynamical

stage. Having a look at the global properties of the sample, we find that our preliminary metallicity-luminosity relation is similar to the one that holds in the Local Group. We do not find any clear trend in median galaxy metallicity versus tidal index (i.e. degree of isolation) or versus distance from the central galaxy of the group.

As a next step in this study, in two companion papers we consider the dwarf irregular galaxies found in the Centaurus A group and for which HST/ACS data are available. Studying dwarf galaxies in Centaurus A and other groups and comparing the results to what we already know about the Local Group will ultimately help us to put further constraints on the connection between star formation, chemical enrichment, and environmental effects on the evolution of dwarf galaxies.

Acknowledgements. D.C. is very thankful to S. Pasetto, K. Glatt, K. Jordi, S. Jin, and T. Lisker for enlightening discussions and useful suggestions. D.C. acknowledges financial support from the MPIA of Heidelberg, as part of the IMPRS program. A.K. acknowledges support by an STFC Postdoctoral Fellowship and by the Heidelberg Graduate School for Fundamental Physics of the University of Heidelberg (grant number GSC 129/1). This work is based on observations made with the NASA/ESA Hubble Space Telescope, obtained from the data archive at the Space Telescope Science Institute. STScI is operated by the Association of Universities for Research in Astronomy, Inc. under NASA contract NAS 5-26555.

References

Armandroff, T. E., Da Costa, G. S., Caldwell, N., & Seitzer, P. 1993, AJ, 106, 986
Banks, G. D., Disney, M. J., Knezek, P. M., et al. 1999, ApJ, 524, 612
Battaglia, G., Tolstoy, E., Helmi, A., et al. 2006, A&A, 459, 423
Belokurov, V., Zucker, D. B., Evans, N. W., et al. 2006, ApJ, 647, L111
Bosler, T. L., Smecker-Hane, T. A., & Stetson, P. B. 2007, MNRAS, 378, 318
Bouchard, A., Jerjen, H., Da Costa, G. S., & Ott, J. 2007, AJ, 133, 261
Bouchard, A., Da Costa, G. S., & Jerjen, H. 2009, AJ, 137, 3038
Boyer, M. L., Skillman, E. D., van Loon, J. T., Gehrz, R. D., & Woodward, C. E. 2009, ApJ, 697, 1993
Coleman, M. G., & de Jong, J. T. A. 2008, ApJ, 685, 933
Côté, S., Freeman, K. C., Carignan, C., & Quinn, P. J. 1997, AJ, 114, 1313
Côté, S., Carignan, C., & Freeman, K. C. 2000, AJ, 120, 3027
Côté, S., Draginda, A., Skillman, E. D., & Miller, B. W. 2009, AJ, 138, 1037
Da Costa, G. S., & Armandroff, T. E. 1990, AJ, 100, 162
Dalcanton, J. J., Williams, B. F., Seth, A. C., et al. 2009, ApJS, 183, 67
Dekel, A., & Silk, J. 1986, ApJ, 303, 39
Dohm-Palmer, R. C., Skillman, E. D., Saha, A., et al. 1997, AJ, 114, 2527
Dolphin, A. E. 2002, MNRAS, 332, 91
Dotter, A., Chaboyer, B., Jevremović, D., et al. 2008, ApJS, 178, 89
Dressler, A. 1980, ApJ, 236, 351
Durrell, P. R., Harris, W. E., & Pritchet, C. J. 2001, AJ, 121, 2557
Einasto, J., Saar, E., Kaasik, A., & Chernin, A. D. 1974, Nature, 252, 111
Gallart, C., Zoccali, M., & Aparicio, A. 2005, ARA&A, 43, 387
Geisler, D., Wallerstein, G., Smith, V. V., & Casetti-Dinescu, D. I. 2007, PASP, 119, 939
Georgiev, I. Y., Goudfrooij, P., Puzia, T. H., & Hilker, M. 2008, AJ, 135, 1858
Gilmore, G., Wilkinson, M. I., Wyse, R. F. G., et al. 2007, ApJ, 663, 948
Girardi, L., Groenewegen, M. A. T., Hatziminaoglou, E., & da Costa, L. 2005, A&A, 436, 895
Glatt, K., Gallagher, III, J. S., Grebel, E. K., et al. 2008a, AJ, 135, 1106
Glatt, K., Grebel, E. K., Sabbi, E., et al. 2008b, AJ, 136, 1703
Goudfrooij, P., Puzia, T. H., Kozhurina-Platais, V., & Chandar, R. 2009, AJ, 137, 4988
Grebel, E. K. 1997, Rev. Mod. Astron. 10, ed. R. E. Schielicke, 29
Grebel, E. K. 2007, in Groups of Galaxies in the Nearby Universe, ed. I. Saviane, V. D. Ivanov, & J. Borissova (Springer), 3
Grebel, E. K., & Gallagher, III, J. S. 2004, ApJ, 610, L89
Grebel, E. K., Seitzer, P., Dolphin, A., et al. 2000, in Stars, Gas and Dust in Galaxies: Exploring the Links, ed. D. Alloin, K. Olsen, & G. Galaz, ASP Conf. Ser., 221, 147
Grebel, E. K., Gallagher, III, J. S., & Harbeck, D. 2003, AJ, 125, 1926
Grossi, M., Disney, M. J., Pritzl, B. J., et al. 2007, MNRAS, 374, 107
Gullieuszik, M., Held, E. V., Saviane, I., & Rizzi, L. 2009, A&A, 500, 735
Han, M., Hoessel, J. G., Gallagher, III, J. S., Holtsman, J., & Stetson, P. B. 1997, AJ, 113, 1001
Harbeck, D., Grebel, E. K., Holtzman, J., et al. 2001, AJ, 122, 3092
Harris, G. L. H., & Harris, W. E. 2000, AJ, 120, 2423
Harris, G. L. H., Harris, W. E., & Poole, G. B. 1999, AJ, 117, 855
Harris, G. L. H., Rejkuba, M., & Harris, W. E. 2009 [arXiv:0911.3180]
Harris, W. E., & Harris, G. L. H. 2002, AJ, 123, 3108
Harris, W. E., Harris, G. L. H., Layden, A. C., & Wehner, E. M. H. 2007, ApJ, 666, 903
Helmi, A., Irwin, M. J., Tolstoy, E., et al. 2006, ApJ, 651, L121
Hui, X., Ford, H. C., Ciardullo, R., & Jacoby, G. H. 1993, ApJ, 414, 463
Hurley-Keller, D., Mateo, M., & Grebel, E. K. 1999, ApJ, 523, L25
Ikuta, C., & Arimoto, N. 2002, A&A, 391, 55
Jerjen, H., Binggeli, B., & Freeman, K. C. 2000a, AJ, 119, 593
Jerjen, H., Freeman, K. C., & Binggeli, B. 2000b, AJ, 119, 166
Kalirai, J. S., Beaton, R. L., Geha, M. C., et al. 2010, ApJ, 711, 671
Karachentsev, I. D. 2005, AJ, 129, 178
Karachentsev, I. D., Sharina, M. E., Dolphin, A. E., et al. 2002, A&A, 385, 21
Karachentsev, I. D., Grebel, E. K., Sharina, M. E., et al. 2003a, A&A, 404, 93
Karachentsev, I. D., Makarov, D. I., Sharina, M. E., et al. 2003b, A&A, 398, 479
Karachentsev, I. D., Sharina, M. E., Dolphin, A. E., et al. 2003c, A&A, 398, 467
Karachentsev, I. D., Karachentseva, V. E., Huchtmeier, W. K., & Makarov, D. I. 2004, AJ, 127, 2031
Karachentsev, I. D., Tully, R. B., Dolphin, A., et al. 2007, AJ, 133, 504
Karachentseva, V. E., & Karachentsev, I. D. 1998, A&AS, 127, 409
King, I. 1962, AJ, 67, 471
Koch, A. 2009, Astron. Nachr., 330, 675
Koch, A., Grebel, E. K., Wyse, R. F. G., et al. 2006, AJ, 131, 895
Koch, A., Grebel, E. K., Kleyna, J. T., et al. 2007a, AJ, 133, 270
Koch, A., Wilkinson, M. I., Kleyna, J. T., et al. 2007b, ApJ, 657, 241
Koch, A., Grebel, E. K., Gilmore, G. F., et al. 2008, AJ, 135, 1580
Koleva, M., de Rijcke, S., Prugniel, P., Zeilinger, W. W., & Michielsen, D. 2009, MNRAS, 396, 2133
Lanfranchi, G. A., & Matteucci, F. 2004, MNRAS, 351, 1338
Lee, H., Zucker, D. B., & Grebel, E. K. 2007, MNRAS, 376, 820
Lee, M. G., Freedman, W. L., & Madore, B. F. 1993, ApJ, 417, 553
Makarova, L., & Makarov, D. 2008, in IAU Symposium, ed. J. Davies, & M. Disney, IAU Symp., 244, 326
Marcolini, A., D'Ercole, A., Brighenti, F., & Recchi, S. 2006, MNRAS, 371, 643
Marcolini, A., D'Ercole, A., Battaglia, G., & Gibson, B. K. 2008, MNRAS, 386, 2173
Marigo, P., Girardi, L., Bressan, A., et al. 2008, A&A, 482, 883
Mateo, M. L. 1998, ARA&A, 36, 435
McLaughlin, D. E., Harris, W. E., & Hanes, D. A. 1994, ApJ, 422, 486
Meier, D. L., Jauncey, D. L., Preston, R. A., et al. 1989, AJ, 98, 27
Mirabel, I. F., Laurent, O., Sanders, D. B., et al. 1999, A&A, 341, 667
Rejkuba, M., Da Costa, G. S., Jerjen, H., Zoccali, M., & Binggeli, B. 2006, A&A, 448, 983
Rejkuba, M., Greggio, L., Harris, W. E., Harris, G. L. H., & Peng, E. W. 2005, ApJ, 631, 262
Renzini, A., & Buzzoni, A. 1986, in Spectral Evolution of Galaxies, ed. C. Chiosi, & A. Renzini, Astrophysics and Space Science Library, 122, 195
Revaz, Y., Jablonka, P., Sawala, T., et al. 2009, A&A, 501, 189
Richardson, J. C., Ferguson, A. M. N., Mackey, A. D., et al. 2009, MNRAS, 396, 1842
Sadakane, K., Arimoto, N., Ikuta, C., et al. 2004, PASJ, 56, 1041
Sarajedini, A., Dotter, A., & Kirkpatrick, A. 2009, ApJ, 698, 1872
Sarajedini, A., Grebel, E. K., Dolphin, A. E., et al. 2002, ApJ, 567, 915
Schlegel, D. J., Finkbeiner, D. P., & Davis, M. 1998, ApJ, 500, 525
Sersic, J. L. 1968, Atlas de galaxias australes
Sharina, M. E., Karachentsev, I. D., Dolphin, A. E., et al. 2008, MNRAS, 384, 1544
Shetrone, M., Venn, K. A., Tolstoy, E., et al. 2003, AJ, 125, 684
Shetrone, M. D., Côté, P., & Sargent, W. L. W. 2001, ApJ, 548, 592
Sirianni, M., Jee, M. J., Benítez, N., et al. 2005, PASP, 117, 1049
Stetson, P. B., Hesser, J. E., & Smecker-Hane, T. A. 1998, PASP, 110, 533
Thomas, D., Bender, R., Hopp, U., Maraston, C., & Greggio, L. 2003, Ap&SS, 284, 599
Tolstoy, E., Hill, V., & Tosi, M. 2009, ARA&A, 47, 371
Tolstoy, E., Irwin, M. J., Helmi, A., et al. 2004, ApJ, 617, L119
Trentham, N., & Tully, R. B. 2002, MNRAS, 335, 712
van den Bergh, S. 1999, A&AR, 9, 273
VandenBerg, D. A., Bergbusch, P. A., & Dowler, P. D. 2006, ApJS, 162, 375
Weisz, D. R., Skillman, E. D., Cannon, J. M., et al. 2008, ApJ, 689, 160
Zucker, D. B., Belokurov, V., Evans, N. W., et al. 2006a, ApJ, 650, L41
Zucker, D. B., Belokurov, V., Evans, N. W., et al. 2006b, ApJ, 643, L103
Zucker, D. B., Kniazev, A. Y., Martínez-Delgado, D., et al. 2007, ApJ, 659, L21